IEEE Access
Multidisciplinary | Rapid Review | Open Access Journal

Received January 18, 2019, accepted February 6, 2019, date of publication February 19, 2019, date of current version March 8, 2019.

Digital Object Identifier 10.1109/ACCESS.2019.2900162

A Novel Power Inversion Antenna Array for the Beidou Navigation Satellite System

YIHENG JIN[1], HAO ZHANG[1,2], (Senior Member, IEEE), TINGTING LU[1], HUA YANG[1], AND T. AARON GULLIVER[2], (Senior Member, IEEE)

[1]Department of Electronic Engineering, Ocean University of China, Qingdao 266100, China
[2]Department of Electrical and Computer Engineering, University of Victoria, Victoria, BC V8W 2Y2, Canada

Corresponding author: Hua Yang (hyang@ouc.edu.cn)

This work was supported in part by the National Natural Science Foundation of China under Grant 61701462, Grant 41527901, Grant 61871354, and Grant 61727806, in part by the Qingdao National Laboratory for Marine Science and Technology under Grant 2017ASKJ01, in part by the Open Studio for Marine High Frequency Communications, Qingdao National Laboratory for Marine Science and Technology, in part by the Pilot National Laboratory for Marine Science and Technology through the Marine S&T Fund of Shandong Province, Qingdao, under Grant 2018SDKJ0210, in part by the Qingdao Science and Technology Plan under Grant 17-1-1-7-jch, in part by the Fundamental Research Funds for the Central Universities under Grant 201713018, and in part by the Natural Science Foundation of Shandong Province under Grant ZR2017MD02.

ABSTRACT Power inversion (PI) arrays have been employed to suppress interference in satellite navigation systems. When the incident direction of a satellite signal is near that of the interference, there will be a significant degradation in the signal to noise ratio (SNR). To reduce this degradation, a PI antenna array composed of a right-hand circular polarized (RHCP) antenna and a spatially-spread electromagnetic vector sensor (SS-EMVS) subarray is proposed, which can suppress interference and acquire satellite signals in both the polarized and spatial domains. Even when the satellite signal is incident from the same direction as the interference, the SNR degradation can be reduced by exploiting the difference in polarization states. It is shown that the filtering is improved in the polarization domain compared with an RHCP PI array, and the SNR loss is lower than with an SS-EMVS PI array while the computational complexity is not increased. Furthermore, the proposed PI array is effective for all Beidou satellite system public service signals.

INDEX TERMS Power inversion array, electromagnetic-vector-sensor, interference suppression, global navigation satellite system.

I. INTRODUCTION

Antenna arrays are widely used for interference suppression in global navigation satellite systems (GNSSs). A power inversion array is an antenna array based on the power inversion (PI) algorithm [1]–[3] to minimize the array output power. With this approach, one antenna element is selected as the reference and the remainder act as auxiliary elements to offset the interference in the reference signal [2]. Typically, the interference is stronger than the satellite signal, but after array processing it is weaker, which is the reason it is called power inversion. A PI array can null interference signals without prior information about the signal structure or direction of arrival (DOA). Further, it is simple to implement and is suitable for acquiring weak signals. This is important because the minimum received power levels for the Beidou navigation satellite (BDS) system public service signals (B1I, B1C, B2a, B3I) are −163 to −156 dBW [4]–[7], which can be much lower than the radio frequency (RF) interference.

BDS navigation signals are right-hand circular polarized (RHCP). Thus to achieve polarization matching, the receiver antenna array elements are also right-hand circular polarized [8], [9]. As a consequence, polarization has been ignored in previous research and PI algorithms have been implemented in only the space [2], [3] or space-time [10]–[12] domains. When the incident direction of a satellite navigation signal is close to that of the interference, there can be significant degradation in the signal to noise ratio (SNR). This is because the spatial resolution of the array is limited by the number of elements regardless of whether interference suppression is employed.

To reduce the SNR degradation, a signal parameter which is independent of the DOA is exploited to separate the signal and interference. An electromagnetic vector sensor (EMVS)

The associate editor coordinating the review of this manuscript and approving it for publication was Xianfu Lei.

array is employed with array signal processing because it can receive incident electromagnetic waves in the form of vectors which include both spatial and polarization domain information [13], [14]. Thus, an EMVS array is also called a polarization sensitive array (PSA) [15], [16]. These arrays have been employed for DOA estimation, polarization estimation, and polarized diversity reception in radar and multiple input multiple output (MIMO) systems [17]–[20]. Compared to arrays with a single type of polarization, an EMVS array provides improved filtering in the polarization domain.

Beamforming and interference suppression using an EMVS array have previously been considered for GNSS receivers. Deterministic beamforming (DBF) and minimum variance distortionless response (MVDR) beamforming were proposed in [21] to enhance the satellite signal. In [22] and [23], joint space-polarization and space-time-polarization arrays were obtained for bi-orthogonal dipoles as array elements. Both solutions increase the signal to interference plus noise ratio (SINR) when the DOA of the satellite signal is similar to that of the interference, but this DOA is required. In [24], a vector sensor array composed of dipoles was used to estimate the DOA of a satellite signal in a multipath environment. Then, MVDR beamforming was employed to suppress the interference and multipath signals. The above approaches all require prior information about the satellite signals to suppress interference in the spatial and polarization domains. The performance of PI based on an EMVS array without this information has not yet been examined for GNSS signals.

In this paper, we propose a PI antenna array with a novel configuration for BDS systems. An RHCP antenna element is employed as a reference to ensure polarization matching with the satellite signals. Other array elements are used to form an EMVS array to improve interference suppression and satellite signal acquisition performance in the polarization domain. The PI algorithm can be directly applied to the array and the computational complexity is not increased compared with traditional RHCP PI arrays. The major contributions of this work are as follows.

1. We develop a mathematical model for the received array signal based on the electromagnetic fields and electromagnetic waves.
2. We verify the effectiveness of the proposed array for interference suppression.
3. We demonstrate the array performance in acquiring satellite signals using the difference in polarization states or DOAs between the signals and interference.
4. We illustrate the effectiveness of the proposed array for BDS public service signals.

The remainder of this paper is organized as follows. The proposed PI array configuration, received signal model, and interference suppression processor are given in Section II. The array is analyzed in Section III. The effectiveness of the proposed PI array is evaluated for BDS public service signals in Section IV. Finally, Section V concludes this paper.

Notation: Superscripts $(\cdot)^T$, $(\cdot)^H$ and $(\cdot)^+$ denote transpose, conjugate transpose, and pseudo-inverse matrix, respectively. Vectors referring to a propagation direction are indicated by $\vec{\bullet}$ and $\vec{e}$ is the unit vector along the subscript coordinate. $\hat{\bullet}$ denotes the maximum likelihood estimator, $\odot$ denotes the Hadamard product, $E\{\cdot\}$ denotes expected value, and $diag\{\cdot\}$ denotes a diagonal matrix. $\boldsymbol{E}_N$ is the identity matrix of size N, $|\cdot|$ denotes the modulus of a complex number, $\angle$ denotes the phase angle of a complex number and $\|\cdot\|^2$ denotes the square of the modulus of a vector.

II. PROPOSED POWER INVERSION ARRAY

A. ARRAY CONFIGURATION

A transverse electromagnetic wave has an electric field vector and a magnetic field vector in the vertical plane of the incident direction. A complete EMVS consists of three orthogonal electric dipoles to measure all components of the electric field vector and three orthogonal magnetic rings to measure all magnetic field components [21]. These components are redundant so a subset can be chosen to form the EMVS array, such as the bi-orthogonal dipole array [22] or the tri-orthogonal dipole array [25]. Dipoles or rings can be spatially collocated or non-collocated in an EMVS. There is no spatial ambiguity between spatially collocated components in an EMVS which is advantageous for DOA estimation, but coupling exists between these components. An EMVS array consisting of orthogonally oriented but spatially non-collocated dipoles or rings is referred to as a spatially-spread EMVS (SS-EMVS) array [13], [21]. This reduces the mutual coupling between dipoles but retains the polarization sensitivity during signal reception.

Figure 1 shows the configuration of the proposed power inversion array. It is a combination of an RHCP antenna and an SS-EMVS subarray. The DOA of the satellite signal is unknown, but its polarization state is RHCP. Therefore, an omnidirectional RHCP antenna is employed as a reference element in the array to provide a constraint on the polarization state of the desired signal. In the SS-EMVS subarray, dipoles with three orthogonal orientations are placed alternately along the y-axis with element spacing d. This subarray can receive all electric field components of an incident signal and is used to suppress the interference and acquire satellite signals in the space-polarization domain. To avoid grating lobes, the array element spacing d is set to $d = \lambda/2$, where λ is the wavelength of the BDS satellite signal.

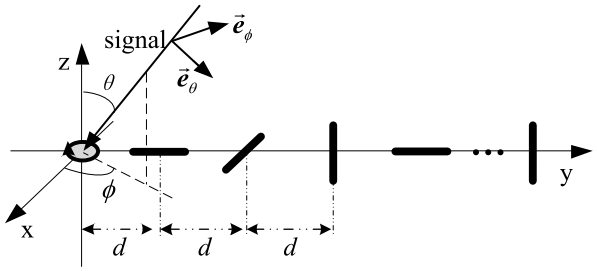

FIGURE 1. Configuration of the proposed power inversion antenna array.

B. RECEIVED ARRAY SIGNAL MODEL

Assume that the combined PI array has N elements. Figure 1 shows that the signal received by each array element is related to its polarization and spatial location. The polarization response of an element to an electromagnetic wave can be described by the polarization steering vector $\boldsymbol{s}_p$. The spatial location of the nth element results in a time delay τ_n relative to the reference antenna. Assuming K interference sources $I_k(t)$, $k = 1, 2, \ldots, K$, and a BDS satellite signal $S_{BDS}(t)$ incident on the array, the received signal can be expressed as

$$\boldsymbol{S}_{sp}(t) = \boldsymbol{s}_{p0} \odot \boldsymbol{S}_{BDS}(t) + \sum_{k=1}^{K} \boldsymbol{s}_{pk} \odot \boldsymbol{I}_k(t) + \boldsymbol{n}(t) \quad (1)$$

where $\boldsymbol{s}_{p0}$ and $\boldsymbol{s}_{pk}$ are the polarization steering vector of the satellite signal and the kth interference signal, respectively. $\boldsymbol{S}_{BDS}(t) = [S_{BDS}(t), \cdots, S_{BDS}(t-\tau_{0n}), \cdots, S_{BDS}(t-\tau_{0N})]^T$ where τ_{0n} is the time delay of the satellite signal received by the nth element. $\boldsymbol{I}_k(t) = [I_k(t), \cdots, I_k(t-\tau_{kn}), \cdots, I_k(t-\tau_{kN})]^T$ where τ_{kn} is time delay of the kth interference signal received by the nth element, and $\boldsymbol{n}(t)$ is additive white Gaussian noise (AWGN) which is assumed to be statistically independent between antenna element channels with identical variance σ^2.

For a narrowband signal $S(t) = s(t)e^{j2\pi f_0 t}$, the variation in the envelope $s(t)$ due to the time delay between array elements can be ignored [12] so that

$$S(t-\tau_n) \approx s(t)e^{j2\pi f_0(t-\tau_n)} \simeq S(t)e^{-j2\pi f_0 \tau_n} \quad (2)$$

We have the following definitions for narrowband signals [26].

Definition 1: $B \ll f_0$ and in general $B/f_0 < 0.1$ where B is the signal bandwidth and f_0 is the center frequency.

Definition 2: $(N-1)d/c \ll 1/B$, where N is the number of elements in the array and c is the speed of light.

The parameters of the BDS public service signals are given in Table 1 [4]–[7]. From Definition 1, $B/f_0 < 0.0208$ for all BDS signals in Table 1, so they can be considered as narrowband signals. According to Definition 2, $N \ll 97.25$ for these signals. Considering array size limitations, $N < 10$ is typical, so the BDS signals can still be considered as narrowband.

TABLE 1. BDS signal parameters.

BDS Signal	Carrier frequency (f_0)	Modulation[a]	Bandwidth (B)
B1I	1561.098 MHz	QPSK	4.092 MHz
B1C	1575.42 MHz	B1C_data: BOC(1,1) B1C_pilot: QMBOC(6,1,4/33)	32.736 MHz
B2a	1176.45 MHz	B2a_data: BPSK(10) B2a_ pilot: BPSK(10)	20.46 MHz
B3I	1268.52 MHz	BPSK(10)	20.46 MHz

[a]QPSK is Quadrature Phase Shift Keying, BOC is Binary Offset Carrier, QMBOC is Quadrature Multiplexed BOC, and BPSK is Binary Phase Shift Keying.

The RF-front end in a BDS receiver will eliminate the spectral components of the received signals which are outside the BDS signal band [27]. Therefore, the maximum interference bandwidth can be considered the same as the satellite signal bandwidth. Thus, the interference can also be considered as narrowband. The received signal in (1) can then be expressed as

$$\begin{aligned}\boldsymbol{S}_{sp}(t) &= \boldsymbol{s}_{p0} \odot \boldsymbol{s}_{s0} S_{BDS}(t) + \sum_{k=1}^{K} \boldsymbol{s}_{pk} \odot \boldsymbol{s}_{sk} I_k(t) + \boldsymbol{n}(t) \\ &= \boldsymbol{s}_{sp0} S_{BDS}(t) + \sum_{k=1}^{K} \boldsymbol{s}_{spk} I_k(t) + \boldsymbol{n}(t) \end{aligned} \quad (3)$$

where $\boldsymbol{s}_{s0} = [1, \cdots, e^{-j2\pi f_0 \tau_{0N}}]^T$ and $\boldsymbol{s}_{sk} = [1, \cdots, e^{-j2\pi f_0 \tau_{kN}}]^T$ are the spatial steering vectors of the satellite signal and the kth interference signal, respectively, and $\boldsymbol{s}_{sp0} = \boldsymbol{s}_{p0} \odot \boldsymbol{s}_{s0}$ and $\boldsymbol{s}_{spk} = \boldsymbol{s}_{pk} \odot \boldsymbol{s}_{sk}$ are the space-polarization steering vectors of the satellite signal and the kth interference signal. The polarization steering vector $\boldsymbol{s}_p$ and the spatial steering vector $\boldsymbol{s}_s$ are derived below.

1) POLARIZATION STEERING VECTOR

Let the DOA of the incident signal be (θ, ϕ) where θ is the pitch angle and ϕ is the azimuth angle. The normalized electric field vector of the signal can be represented as [13], [21]

$$\vec{E} = E_\theta \vec{\boldsymbol{e}}_\theta + E_\phi \vec{\boldsymbol{e}}_\phi = \cos\gamma \vec{\boldsymbol{e}}_\theta + \sin\gamma e^{j\eta} \vec{\boldsymbol{e}}_\phi \quad (4)$$

where $E_\theta = \cos\gamma$ and $E_\phi = \sin\gamma e^{j\eta}$ are orthogonal electric field components in the vertical plane of the incident direction, and $\gamma \in [0°, 90°]$ and $\eta \in [-180°, 180°]$ are the polarization angles of the incident signal. Figure 2 shows the correspondence between E_θ/E_ϕ and the polarization state for an electromagnetic wave. It can be seen from (4) and Figure 2 that the incident signal is linear polarized (LP) when $\eta = 0°$ or $\eta = \pm 180°$, left-hand circular polarized (LHCP) when $\gamma = 45°$ and $\eta = 90°$, and RHCP when $\gamma = 45°$ and $\eta = -90°$. For other values of (γ, η), the signal is

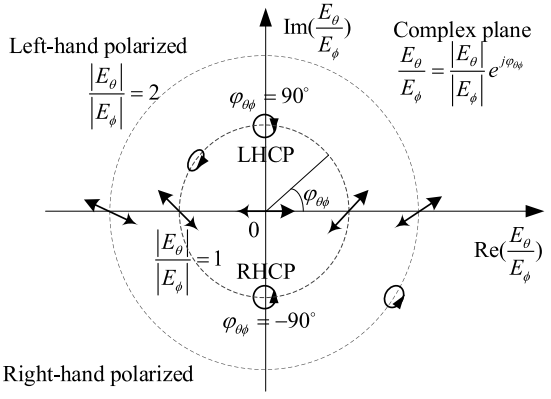

FIGURE 2. Correspondence between the polarization state and the orthogonal electric field components for an electromagnetic wave.

elliptically polarized. Further, the signal is left-hand polarized when $\eta > 0°$ and right-hand polarized when $\eta < 0°$.

The electric field vector $\vec{E}$ can be expressed in rectangular coordinates as

$$\vec{E} = E_x\vec{e}_x + E_y\vec{e}_y + E_z\vec{e}_z \tag{5}$$

and the three orthogonal electric field components are [13]

$$\begin{bmatrix} E_x \\ E_y \\ E_z \end{bmatrix} = \begin{bmatrix} -\sin\phi & \cos\theta\cos\phi \\ \cos\phi & \cos\theta\sin\phi \\ 0 & -\sin\theta \end{bmatrix} \begin{bmatrix} \cos\gamma \\ \sin\gamma e^{j\eta} \end{bmatrix} \tag{6}$$

E_x, E_y, and E_z are received by the dipoles placed along the x-axis, y-axis and z-axis, respectively. Thus, based on the SS-EMVS subarray as shown in Figure 1, the polarization steering vector of the incident signal can be expressed as

$$\tilde{\boldsymbol{s}}_{p\_sub}(\theta, \varphi, \gamma, \eta) = \left[\underbrace{E_y, E_x, E_z, E_y, E_x, \cdots, E_z}_{N-1}\right]^T \tag{7}$$

Assume that the polarization steering element based on the reference RHCP antenna is s_{p_ref}. In previous research on RHCP PI arrays, the interference polarization was not considered in the received signal model [2], [3], i.e. s_{p_ref} was ignored. Typically, when an RHCP antenna receives a signal with a different polarization, signal power is lost due to polarization mismatch. Thus, s_{p_ref} should be included to reflect this mismatch.

An arbitrary electromagnetic wave can be decomposed into an RHCP wave and an LHCP wave. According to Figure 2, the electric field vectors of RHCP and LHCP waves can be expressed as [28]

$$\vec{E}_{RHCP} = E_{RHCP}\vec{\boldsymbol{e}}_R = \frac{1}{\sqrt{2}}(\vec{\boldsymbol{e}}_\theta - j\vec{\boldsymbol{e}}_\phi)E_{RHCP} \tag{8}$$

$$\vec{E}_{LHCP} = E_{LHCP}\vec{\boldsymbol{e}}_L = \frac{1}{\sqrt{2}}(\vec{\boldsymbol{e}}_\theta + j\vec{\boldsymbol{e}}_\phi)E_{LHCP} \tag{9}$$

where E_{RHCP} and E_{LHCP} are the complex electric field amplitude of the RHCP wave and LHCP wave, respectively, and $\vec{\boldsymbol{e}}_R$ and $\vec{\boldsymbol{e}}_L$ are the unit electric field vectors of these waves. Therefore, (5) can be rewritten as

$$\begin{aligned} \vec{E} &= \vec{E}_{RHCP} + \vec{E}_{LHCP} \\ &= \frac{\sqrt{2}}{2}(\cos\gamma + j\sin\gamma e^{j\eta})\vec{\boldsymbol{e}}_R \\ &\quad + \frac{\sqrt{2}}{2}(\cos\gamma - j\sin\gamma e^{j\eta})\vec{\boldsymbol{e}}_L \end{aligned} \tag{10}$$

Polarization isolation exists between the RHCP antenna and the LHCP wave. Thus, only $\vec{E}_{RHCP}$ in the above equation is received by the RHCP antenna. The received electric field components at the reference RHCP antenna are

$$E_{RHCP} = \frac{\sqrt{2}}{2}(\cos\gamma + j\sin\gamma e^{j\eta}) \tag{11}$$

With an omnidirectional RHCP antenna, s_{p_ref} is independent of (θ, ϕ) so

$$s_{p\_ref}(\gamma, \eta) = E_{RHCP} = \frac{\sqrt{2}}{2}(\cos\gamma + j\sin\gamma e^{j\eta}) \tag{12}$$

s_{p_ref} is 1 for an RHCP signal with $(\gamma, \eta) = (45°, -90°)$ and 0 for an LHCP signal with $(\gamma, \eta) = (45°, 90°)$.

In order to reflect the power loss during signal reception by the reference antenna, define the polarization matching factor as

$$\alpha = \frac{\left|\vec{E}_{RHCP}\right|^2}{\left|\vec{E}\right|^2} = \left|s_{p\_ref}\right|^2 = \frac{1}{2}(1 - \sin 2\gamma \sin\eta) \tag{13}$$

where $\left|\vec{E}\right|^2 = 1$ and $\alpha \in [0, 1]$. A large α indicates low power loss and better polarization matching between the RHCP antenna and incident signal. α is 1 for an RHCP signal, which indicates that there is no power loss during reception. The polarization steering vector of the combined PI array is then

$$\begin{aligned} \boldsymbol{s}_p(\theta, \varphi, \gamma, \eta) &= \left[s_{p\_ref}, \underbrace{E_y, E_x, E_z, E_y, \cdots}_{N-1}\right]^T \\ &= \begin{bmatrix} s_{p\_ref} \\ \tilde{\boldsymbol{s}}_{p\_sub} \end{bmatrix} \end{aligned} \tag{14}$$

2) SPATIAL STEERING VECTOR

As shown in Figure 1, the reference element is placed at the origin of the coordinate system, and the coordinates of the nth antenna element are $\boldsymbol{l}_n = (0, (n-1)d, 0)^T$. The time delay τ_n in (1) is

$$\tau_n = \frac{\boldsymbol{k}\boldsymbol{l}_n}{c} \tag{15}$$

where $\boldsymbol{k}$ is the beam vector of the incident signal given by $\boldsymbol{k} = [\sin\theta\cos\phi \ \sin\theta\sin\phi \ \cos\theta]$.

From the previous analysis, the signal propagation time delay can be replaced by the corresponding phase delay. The phase delay of the signal received by the nth element relative to the reference antenna is

$$\Phi_n = -2\pi f_0\tau_n = -\frac{2\pi}{\lambda}\sin\theta\sin\phi(n-1)d \tag{16}$$

The spatial steering vector of the incident signal is

$$\boldsymbol{s}_s(\theta, \phi) = [1 \ e^{j\Phi_2} \ \cdots \ e^{j\Phi_N}]^T = \begin{bmatrix} 1 \\ \tilde{\boldsymbol{s}}_{s\_sub} \end{bmatrix} \tag{17}$$

where $\tilde{\boldsymbol{s}}_{s\_sub} = [e^{j\Phi_2}, \cdots, e^{j\Phi_N}]^T$ is the spatial steering vector based on the SS-EMVS subarray.

C. INTERFERENCE SUPPRESSION PROCESSOR

Figure 3 gives the structure of the space-polarization processor for interference suppression. The signal received at each antenna element is weighted so the output is

$$y(t) = \boldsymbol{w}^H\boldsymbol{S}_{sp}(t) \tag{18}$$

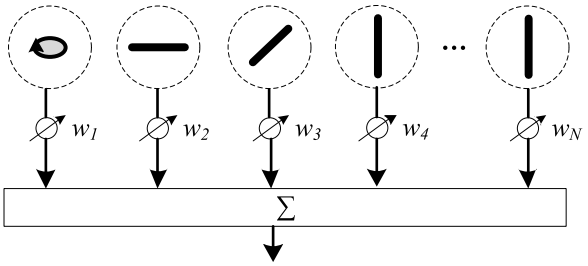

FIGURE 3. The structure of the space-polarization processor for interference suppression.

where $\boldsymbol{w} = [w_1, w_2, \cdots, w_N]$ is the weight vector. The output power is

$$P_{\text{out}} = E\left\{|y(t)|^2\right\} = E\left\{\boldsymbol{w}^H \boldsymbol{R}_{xx} \boldsymbol{w}\right\} \tag{19}$$

where $\boldsymbol{R}_{xx} = E\left\{\boldsymbol{S}_{sp}(t)\boldsymbol{S}_{sp}^H(t)\right\}$ is the covariance matrix of the received signal $\boldsymbol{S}_{sp}(t)$. The principle of the PI algorithm is to set the weight of the reference antenna to 1 and choose the other weights to minimize the output power. The optimization problem is then

$$\begin{cases} \min \ \ \boldsymbol{w}^H \boldsymbol{R}_{xx} \boldsymbol{w} \\ s.t. \ \ \boldsymbol{w}(1) = 1 \end{cases} \tag{20}$$

The weight vector can be written as

$$\boldsymbol{w} = [\,1 \ w_2 \ w_3 \ \cdots w_N\,]^H = \begin{bmatrix} 1 \\ \tilde{\boldsymbol{w}} \end{bmatrix} \tag{21}$$

where $\tilde{\boldsymbol{w}} = [\,w_2 \ w_3 \ \cdots w_N\,]^H$, so $\boldsymbol{S}_{sp}(t)$ can be expressed as

$$\boldsymbol{S}_{sp}(t) = \begin{bmatrix} S_{sp1}(t) \\ \tilde{\boldsymbol{S}}_{sp}(t) \end{bmatrix} \tag{22}$$

where $S_{sp1}(t)$ is the received signal at the reference antenna and $\tilde{\boldsymbol{S}}_{sp}(t)$ is the SS-EMVS subarray received signal vector.

$\boldsymbol{R}_{xx}$ can be written in block matrix form as

$$\boldsymbol{R}_{xx} = \begin{bmatrix} R & \boldsymbol{R}_2 \\ \boldsymbol{R}_3 & \tilde{\boldsymbol{R}} \end{bmatrix} \tag{23}$$

where $R = E\left\{S_{sp1}(t)S_{sp1}^H(t)\right\}$, $\boldsymbol{R}_2 = E\left\{S_{sp1}(t)\tilde{\boldsymbol{S}}_{sp}^H(t)\right\}$, $\boldsymbol{R}_3 = E\left\{\tilde{\boldsymbol{S}}_{sp}(t)S_{sp1}^H(t)\right\}$, and $\tilde{\boldsymbol{R}} = E\left\{\tilde{\boldsymbol{S}}_{sp}(t)\tilde{\boldsymbol{S}}_{sp}^H(t)\right\}$. The output power can then be expressed as

$$\begin{aligned} \boldsymbol{w}^H \boldsymbol{R}_{xx} \boldsymbol{w} &= \begin{bmatrix} 1 & \tilde{\boldsymbol{w}}^H \end{bmatrix} \begin{bmatrix} R & \boldsymbol{R}_2 \\ \boldsymbol{R}_3 & \tilde{\boldsymbol{R}} \end{bmatrix} \begin{bmatrix} 1 \\ \tilde{\boldsymbol{w}} \end{bmatrix} \\ &= R + \tilde{\boldsymbol{w}}^H \boldsymbol{R}_3 + \boldsymbol{R}_2 \tilde{\boldsymbol{w}} + \tilde{\boldsymbol{w}}^H \tilde{\boldsymbol{R}} \tilde{\boldsymbol{w}} \end{aligned} \tag{24}$$

Taking the partial derivative and setting it to zero

$$\frac{\partial}{\tilde{\boldsymbol{w}}} \boldsymbol{w}^H \boldsymbol{R}_{xx} \boldsymbol{w} = \boldsymbol{R}_2^H + \boldsymbol{R}_3 + 2\tilde{\boldsymbol{R}}\tilde{\boldsymbol{w}} = 0 \tag{25}$$

from (23) gives that $\boldsymbol{R}_2^H = \boldsymbol{R}_3$. Therefore, the optimal weight vector is

$$\tilde{\boldsymbol{w}}_{opt} = -\tilde{\boldsymbol{R}}^{-1} \boldsymbol{R}_3 \tag{26}$$

The optimal weight vector for array space-polarization PI (SP-PI) processing is

$$\boldsymbol{w}_{opt} = \begin{bmatrix} 1 \\ \tilde{\boldsymbol{w}}_{opt} \end{bmatrix} \tag{27}$$

III. ARRAY BEHAVIOR

A traditional RHCP PI array and an SS-EMVS PI array are shown in Figure 4. They are used in this section to evaluate the performance of the combined PI array. The arrays have the same number of elements N and element spacing d. The subarray elements of the SS-EMVS array are arranged in the same way as the subarray of the combined PI array. The first elements of the two arrays are selected as the reference elements. For the RHCP PI array, the polarization steering vector is $\boldsymbol{s}_p = [s_{p\_ref}, \cdots, s_{p\_ref}]^T$, the subarray polarization steering vector is $\tilde{\boldsymbol{s}}_{p\_sub} = \left[\underbrace{s_{p\_ref}, \cdots, s_{p\_ref}}_{N-1}\right]^T$ and the polarization matching factor for the reference antenna is $\alpha = \left|s_{p\_ref}\right|^2$. For the SS-EMVS PI array, there are three options for the orientation of the reference dipole. We place the reference dipole along the x-axis so that $s_{p\_ref} = E_x$, $\alpha = |E_x|^2$, and $\boldsymbol{s}_p = [E_x, E_y, E_x, E_z, E_y, \cdots, E_z]^T$ for the SS-EMVS PI array.

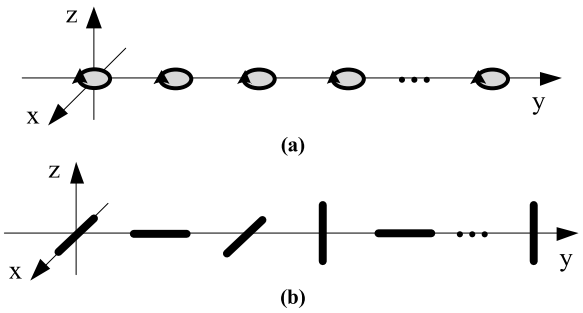

FIGURE 4. Configuration of two traditional PI arrays. (a) RHCP PI array and (b) SS-EMVS PI array.

Assuming the satellite signal, interference and noise are independent of each other. $\boldsymbol{R}_{xx}$ in (22) can be written as

$$\boldsymbol{R}_{xx} = \boldsymbol{R}_s + \boldsymbol{R}_i + \boldsymbol{R}_n \tag{28}$$

where $\boldsymbol{R}_s, \boldsymbol{R}_i$, and $\boldsymbol{R}_n$ are the covariance matrices of the signal, interference, and noise, respectively. They can be expressed as

$$\begin{aligned} \boldsymbol{R}_s &= E\{(\boldsymbol{s}_{p0} \odot \boldsymbol{S}_{BDS}(t))(\boldsymbol{s}_{p0} \odot \boldsymbol{S}_{BDS}(t))^H\} \\ &= P_0 \boldsymbol{s}_{sp0} \boldsymbol{s}_{sp0}^H \end{aligned} \tag{29}$$

$$\begin{aligned} \boldsymbol{R}_i &= \sum_{k=1}^{K} E\{(\boldsymbol{s}_{pk} \odot \boldsymbol{I}_k(t))(\boldsymbol{s}_{pk} \odot \boldsymbol{I}_k(t))^H\} \\ &= \sum_{k=1}^{K} P_k \boldsymbol{s}_{spk} \boldsymbol{s}_{spk}^H \end{aligned} \tag{30}$$

$$\boldsymbol{R}_n = E\{\boldsymbol{n}(t)\boldsymbol{n}(t)^H\} = \sigma^2 \boldsymbol{E}_N \tag{31}$$

where P_0 is the satellite signal power, P_k is the power of the kth interferer, and σ^2 is the noise power. $\boldsymbol{R}_3$ and $\tilde{\boldsymbol{R}}$ in (26) are given by

$$\boldsymbol{R}_3 = P_0\tilde{\boldsymbol{s}}_{sp\_sub0}s^H_{p\_ref0} + \sum_{k=1}^{K} P_k\tilde{\boldsymbol{s}}_{sp\_subk}s^H_{p\_refk} \tag{32}$$

$$\tilde{\boldsymbol{R}} = P_0\tilde{\boldsymbol{s}}_{sp\_sub0}\tilde{\boldsymbol{s}}^H_{sp\_sub0} + \sum_{k=1}^{K} P_k\tilde{\boldsymbol{s}}_{sp\_subk}\tilde{\boldsymbol{s}}^H_{sp\_subk} + \sigma^2\boldsymbol{E}_{N-1} \tag{33}$$

where s_{p_ref0} and $\tilde{\boldsymbol{s}}_{sp\_sub0}$ are the first and second to Nth elements of $\boldsymbol{s}_{sp0}$, respectively, and s_{p_refk} and $\tilde{\boldsymbol{s}}_{sp\_subk}$ are the first and second to Nth elements of $\boldsymbol{s}_{spk}$.

Assume that the satellite signal is incident from the direction (θ_0, ϕ_0) with $(\gamma_0, \eta_0) = (45°, -90°)$ and the kth interference signal is incident from the direction (θ_k, ϕ_k) with polarization angles (γ_k, η_k). To simplify the following analysis, some of these parameters are fixed.

A. INTERFERENCE SUPPRESSION

In general, the power of GNSS satellite signals is much lower than that of the thermal noise thus can be ignored when calculating R_{xx} [12]. Assuming a single interference signal incident on the array, $\boldsymbol{R}_3$ and $\tilde{\boldsymbol{R}}$ in (26) can be approximated as

$$\tilde{\boldsymbol{R}} \approx \sigma^2\boldsymbol{E}_{N-1} + P_1\tilde{\boldsymbol{s}}_{sp\_sub1}\tilde{\boldsymbol{s}}^H_{sp\_sub1} \tag{34}$$

$$\boldsymbol{R}_3 \approx P_1\tilde{\boldsymbol{s}}_{sp\_sub1}s^H_{p\_ref1} \tag{35}$$

From the matrix inversion lemma [12]

$$\tilde{\boldsymbol{R}}^{-1} \approx \frac{1}{\sigma^2}[\boldsymbol{E}_{N-1} - \frac{P_1\tilde{\boldsymbol{s}}_{sp\_sub1}\tilde{\boldsymbol{s}}^H_{sp\_sub1}}{\sigma^2 + P_1\left\|\tilde{\boldsymbol{s}}_{sp\_sub1}\right\|^2}] \tag{36}$$

where $\left\|\tilde{\boldsymbol{s}}_{sp\_sub1}\right\|^2 = \tilde{\boldsymbol{s}}^H_{sp\_sub1}\tilde{\boldsymbol{s}}_{sp\_sub1}$. Thus $\tilde{\boldsymbol{w}}_{opt}$ can be given as

$$\tilde{\boldsymbol{w}}_{opt} = -\tilde{\boldsymbol{R}}^{-1}\boldsymbol{R}_3 \approx -\frac{s^H_{p\_ref1}}{1 + INR_1\left\|\tilde{\boldsymbol{s}}_{sp\_sub1}\right\|^2}\tilde{\boldsymbol{s}}_{sp\_sub1} \tag{37}$$

where $INR_1 = P_1/\sigma^2$ is the interference to noise ratio (INR) of the incident interference signal. The interference signal power at the output of the array is

$$\begin{aligned} P_{1out} &= E\left\{\left|\boldsymbol{w}^H_{opt}\boldsymbol{I}_1(t)\right|^2\right\} \\ &= E\left\{\left|(s_{p\_ref1} - \tilde{\boldsymbol{w}}^H_{opt}\tilde{\boldsymbol{s}}_{sp\_sub1})I_1(t)\right|^2\right\} \\ &\approx P_1\alpha_1\left(\frac{1}{1 + INR_1\left\|\tilde{\boldsymbol{s}}_{sp\_sub1}\right\|^2}\right)^2 \end{aligned} \tag{38}$$

where $\alpha_1 = \left|s_{p\_ref1}\right|^2$ is the polarization matching factor of the incident interference signal.

The purpose of interference suppression is to reduce P_{1out}, i.e. make the weighted output of the subarray offset the interference in the reference signal. From (38), P_{1out} is a function of P_1, INR_1, α_1, and $\boldsymbol{s}_{p1}$. First, P_{1out} is close to 0 if α_1 is close to 0, and for an LHCP interferer with $\alpha_1 = 0$, P_{1out} is 0. Then $\tilde{\boldsymbol{w}}_{opt}$ is approximately 0 according to (37), and when the interference signal power received by the reference antenna is 0, the offset provided by the subarray is unnecessary. Second, for interferers with $\alpha_1 \neq 0$, the larger $INR_1\left\|\tilde{\boldsymbol{s}}_{sp\_sub1}\right\|^2$ is, the closer P_{1out} is to 0.

1) NECESSITY OF THREE DIPOLE ORIENTATIONS

According to the above analysis, P_{1out} decreases to 0 as $INR_1\left\|\tilde{\boldsymbol{s}}_{sp\_sub1}\right\|^2$ increases when $\alpha_1 \neq 0$. However, if $\left\|\tilde{\boldsymbol{s}}_{sp\_sub1}\right\|^2$ is 0, P_{1out} is approximately equal to $P_1\alpha_1$, which is the power of the interference signal received by the reference antenna. Hence, $\left\|\tilde{\boldsymbol{s}}_{sp\_sub1}\right\|^2$ should not be 0. The value of $\left\|\tilde{\boldsymbol{s}}_{sp\_sub1}\right\|^2$ is related to the number and configuration of dipoles in the subarray. Considering dipoles placed as shown in Figure 1, $\left\|\tilde{\boldsymbol{s}}_{sp\_sub1}\right\|^2$ can be obtained as

$$\left\|\tilde{\boldsymbol{s}}_{sp\_sub1}\right\|^2 = \begin{cases} \left|E_y\right|^2 \le 1 - \sin^2\theta_1\sin^2\phi_1, & N-1=1 \\ \left|E_y\right|^2 + \left|E_x\right|^2 = 1 - \sin^2\theta_1\sin^2\gamma_1, & N-1=2 \\ \left|E_y\right|^2 + \left|E_x\right|^2 + \left|E_z\right|^2 = 1, & N-1=3 \\ 1 + \left|E_y\right|^2, & N-1=4 \\ \vdots & \\ \dfrac{N-1}{3}, & N-1=3 \times(2,3,\cdots) \end{cases} \tag{39}$$

where $N-1$ is the number of dipoles in the subarray. When $N-1=1$, zero values of $\left\|\tilde{\boldsymbol{s}}_{sp\_sub1}\right\|^2$ occur at $(\theta_1, \phi_1) = (90°, 90°)$, $(\phi_1, \gamma_1) = (0°, 90°)$ and $(\phi_1, \gamma_1) = (90°, 0°)$. When $N-1=2$, zero values of $\left\|\tilde{\boldsymbol{s}}_{sp\_sub1}\right\|^2$ occur at $(\theta_1, \gamma_1) = (90°, 90°)$. When $N-1 \ge 3$, $\left\|\tilde{\boldsymbol{s}}_{sp\_sub1}\right\|^2$ has no zero values. The zero values occur because a single dipole or two dipoles can only receive a subset of the three electric field components. If the electric field vector of the interference signal is perpendicular to all axes of the dipoles, the subarray receives no electric field components. That is, the weighted output of the subarray cannot offset the interference component in the reference signal. Therefore, to suppress an interference signal with arbitrary polarization state and DOA, at least one set of three oriented dipoles should be contained in the subarray.

2) EFFECT OF THE NUMBER OF ELEMENTS AND INTERFERENCE PARAMETERS

Normalizing the interference signal power at the output of the array to P_{1out}/σ^2, from (38) P_{1out}/σ^2 is determined by INR_1, α_1 and $\left\|\tilde{\boldsymbol{s}}_{sp\_sub1}\right\|^2$. The values of $\left\|\tilde{\boldsymbol{s}}_{sp\_sub1}\right\|^2$ are equal for the combined PI array and the SS-EMVS PI array as shown in (39). The values of α_1 are equal for the combined PI array and the RHCP PI array, which range from 0 to 1 and are

determined by (γ_1, η_1). Further, $\alpha_1 = |E_x(\theta_1, \phi_1, \gamma_1, \eta_1)|^2$ for the SS-EMVS PI array with values from 0 to 1, and $\left\|\tilde{\boldsymbol{s}}_{sp\_sub1}\right\|^2 = N\alpha_1$ for the RHCP PI array.

The number of array elements is set to $N \geq 4$ in order to contain at least one set of three oriented dipoles. Figure 5 shows P_{1out}/σ^2 versus N, INR_1 and α_1 with the combined PI array, RHCP PI array and SS-EMVS PI array. Figure 5(a) indicates that P_{1out}/σ^2 of the interferer with $(\theta_1, \phi_1, \gamma_1, \eta_1) = (40°, 90°, 45°, 10°)$ decreases as the number of array elements N increases for these three arrays. This is because the value of $\left\|\tilde{\boldsymbol{s}}_{sp\_sub1}\right\|^2$ increases as N increases for all arrays. Figure 5(b) indicates that P_{1out}/σ^2 decreases linearly as INR_1 increases for the three arrays with $INR_1 >$ 0 dB. When INR_1 is lower than -5 dB, P_{1out}/σ^2 increases as INR_1 increases, but is lower than the corresponding INR_1. The greater the interference power is, the stronger the suppression is. This is a characteristic of PI arrays. In Figure 5(c), N is set to be 7, thus values of $\left\|\tilde{\boldsymbol{s}}_{sp\_sub1}\right\|^2$ for the three arrays are independent of the signal DOA. For an interferer with arbitrary DOA and arbitrary polarization angles, P_{1out}/σ^2 is determined by α_1. The combined PI array has the same P_{1out}/σ^2 as the SS-EMVS PI array with the same α_1. For the combined PI array, P_{0out}/σ^2 increases as α_1 increases with the maximum value lower than -55 dB. For the RHCP PI array, $\left\|\tilde{\boldsymbol{s}}_{sp\_sub1}\right\|^2$ is determined by α_1 and the maximum value of P_{1out}/σ^2 occurs with $\alpha_1 = 1/(N \times INR_1)$. This maximum value is larger than -30 dB as shown in Figure 5(c). In addition, the combined PI array has a higher P_{1out}/σ^2 than the RHCP PI array with $\alpha_1 > 0.33$, but the difference is insignificant since -55 dB is close to 0.

In summary, the combined PI array provides better interference suppression with a larger N, a larger INR_1 or a smaller α_1. Further, over the entire range of α_1, the combined array provides more stable interference suppression than the RHCP PI array.

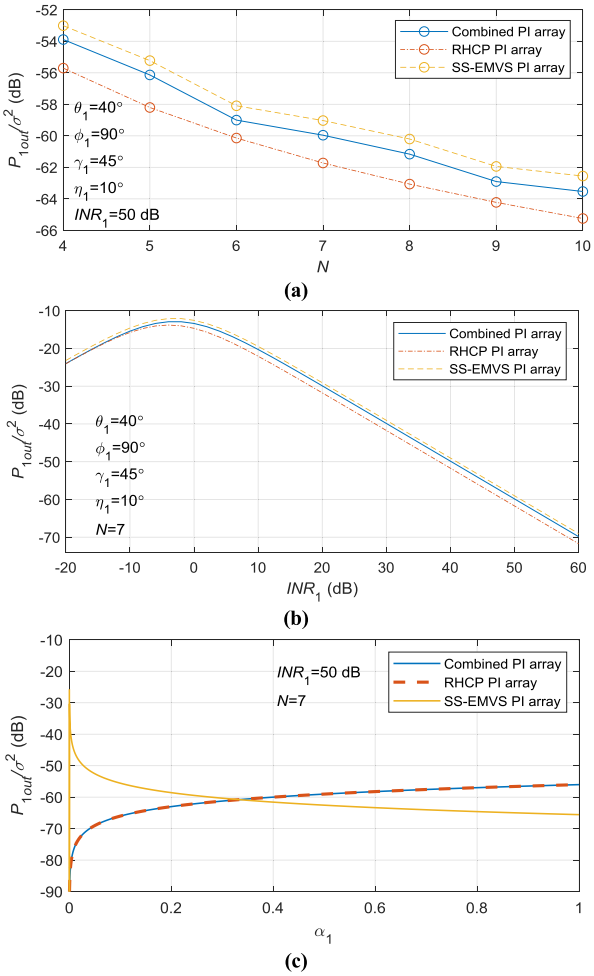

FIGURE 5. P_{1out}/σ^2 of the combined PI array, RHCP PI array and SS-EMVS PI array. (a) P_{1out}/σ^2 versus the number of array elements N, (b) P_{1out}/σ^2 versus INR_1, and (c) P_{1out}/σ^2 versus α_1.

B. SATELLITE SIGNAL ACQUISITION

Assuming a single interference signal incident on the array, the satellite signal at the output of the array is

$$S_{BDSout}(t) = \boldsymbol{w}_{opt}^H \boldsymbol{S}_{BDS}(t) = (s_{p\_ref0} + \tilde{\boldsymbol{w}}_{opt}^H \tilde{\boldsymbol{s}}_{sp\_sub0}) S_{BDS}(t) \tag{40}$$

The output satellite signal power is then

$$\begin{aligned} P_{0out} &= E\left\{|S_{BDSout}(t)|^2\right\} \\ &\approx P_0\alpha_0 \left| 1 - \frac{INR_1}{1 + INR_1 \left\|\tilde{\boldsymbol{s}}_{sp\_sub1}\right\|^2} \right. \\ &\quad \left. \times \frac{s_{p\_ref1}}{s_{p\_ref0}} \tilde{\boldsymbol{s}}_{sp\_sub1}^H \tilde{\boldsymbol{s}}_{sp\_sub0} \right|^2 \end{aligned} \tag{41}$$

where $\alpha_0 = \left|s_{p\_ref0}\right|^2$ is the polarization matching factor of this signal. From (40) and (41), the satellite signal is also weighted during interference suppression which is the cause of the SNR degradation for PI arrays. To evaluate this degradation, the SNR loss is defined as

$$\begin{aligned} SNR_{loss} &= SNR\ (\text{dB}) - SNR_{out} \\ (\text{dB}) &= 10 \log \frac{SNR}{SNR_{out}}\ (\text{dB}) \end{aligned} \tag{42}$$

where $SNR = P_0/\sigma^2$ is the SNR at the input of the array, $SNR_{out} = P_{0out}/P_{\sigma out}$ is the SNR at the output of the array, and $P_{\sigma out}$ is the noise power at the output of the array with

$$\begin{aligned} P_{\sigma out} &= E\left\{ \left| \left[1,\ \tilde{\boldsymbol{w}}_{opt}^H\right] \boldsymbol{n}(t) \right|^2 \right\} \\ &\approx \sigma^2 \left[1 + \alpha_1 \frac{INR_1^2 \left\|\tilde{\boldsymbol{s}}_{sp\_sub1}\right\|^2}{(1 + INR_1 \left\|\tilde{\boldsymbol{s}}_{sp\_sub1}\right\|^2)^2} \right] \end{aligned} \tag{43}$$

According to the analysis above, the output interference signal power is approximately 0. Thus, a lower SNR loss indicates better signal acquisition performance at the output of the array. From (43), $P_{\sigma out}$ is determined by $\boldsymbol{s}_{sp1}$. From (41), P_{0out} is determined by $\boldsymbol{s}_{sp1}$ and $\boldsymbol{s}_{sp0}$ as well as the proximity

of $\boldsymbol{s}_{sp1}$ and $\boldsymbol{s}_{sp0}$. In particular, P_{0out} is approximately 0 when $\boldsymbol{s}_{sp1}$ is equal to $\boldsymbol{s}_{sp0}$. This corresponds to a significant SNR loss when the satellite signal and the interference signal have the same DOA and polarization angles. However, $P_{0out} \neq 0$ with $\boldsymbol{s}_{sp1} \neq \boldsymbol{s}_{sp0}$, which indicates that the array can acquire the satellite signal as long as the DOA or polarization state of the satellite signal is different from that of the interference.

1) SIGNAL ACQUISITION IN POLARIZATION DOMAIN

Assume that the interference has the same DOA as the satellite signal and $P_1 \gg \sigma^2$, and the number of subarray elements $N-1$ is a multiple of 3. For the combined PI array

$$\begin{aligned}
&\tilde{\boldsymbol{s}}_{sp_sub1}^H \tilde{\boldsymbol{s}}_{sp_sub0} \\
&\quad = \tilde{\boldsymbol{s}}_{p_sub}^H(\theta, \phi, \gamma_1, \eta_1)\tilde{\boldsymbol{s}}_{p_sub}(\theta, \phi, 45^\circ, -90^\circ) \\
&\quad = \frac{N-1}{3}\left(\begin{bmatrix}\cos\gamma_1 \\ \sin\gamma_1 e^{j\eta_1}\end{bmatrix}^H \begin{bmatrix}\cos 45^\circ \\ \sin 45^\circ e^{-j90^\circ}\end{bmatrix}\right) \\
&\quad = \frac{N-1}{3}\frac{\sqrt{2}}{2}(\cos\gamma_1 - j\sin\gamma_1 e^{-j\eta_1}) \qquad (44)
\end{aligned}$$

As $s_{p\_ref0} = 1$ and $\alpha_0 = 1$, P_{0out} can be approximated as

$$\begin{aligned}
P_{0out} &\approx P_0 \left| 1 - s_{p_ref1} \frac{\tilde{\boldsymbol{s}}_{sp_sub1}^H \tilde{\boldsymbol{s}}_{sp_sub0}}{\left\| \tilde{\boldsymbol{s}}_{sp_sub1} \right\|^2} \right|^2 \\
&= \frac{P_0}{4}(1 + \sin 2\gamma_1 \sin\eta_1)^2 \\
&= P_0(1-\alpha_1)^2 \qquad (45)
\end{aligned}$$

Equation (45) indicates that the satellite signal power after array processing is determined by α_1. For an interferer with an arbitrary polarization angle, the value of P_{0out} ranges from 0 to P_0. In particular, P_{0out} is 0 for RHCP interferers with $\alpha_1 = 1$.

$P_{\sigma out}$ can be simplified as

$$P_{\sigma out} \approx \sigma^2 \left[1 + \alpha_1 \frac{3}{N-1} \right] \qquad (46)$$

which indicates that $P_{\sigma out}$ ranges from σ^2 to $\sigma^2(1+3/(N-1))$. In particular, P_{0out} is σ^2 for LHCP interferers and $\sigma^2(1+3/(N-1))$ for RHCP interferers. Further, the maximum value of $P_{\sigma out}$ decreases as N increases. The SNR loss is

$$SNR_{loss} \approx 10\lg \frac{1 + \alpha_1 \frac{3}{N-1}}{(1-\alpha_1)^2} \text{ (dB)} \qquad (47)$$

From (47), SNR_{loss} of the combined PI array is a function of α_1. Figure 6 shows SNR_{loss} versus α_1 for the combined PI array with $N = 7$. The SNR loss is 0 dB for LHCP interferers and larger than 0 dB for interferers with other polarization angles. In addition, SNR_{loss} increases as α_1 increases. This indicates that the closer the polarization state of an interferer is to RHCP, the larger the SNR loss. In summary, when suppressing interference incident from the same direction but with different polarization angles, an SNR loss occurs but the satellite signal is not completely eliminated.

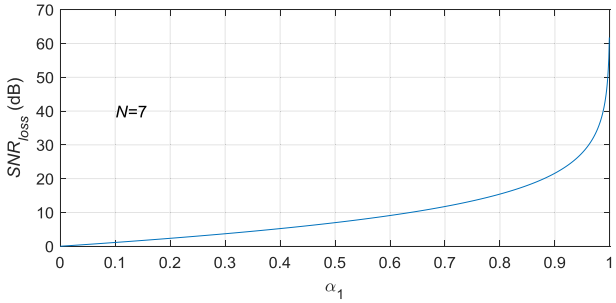

FIGURE 6. SNR_{loss} versus α_1 for the combined PI array.

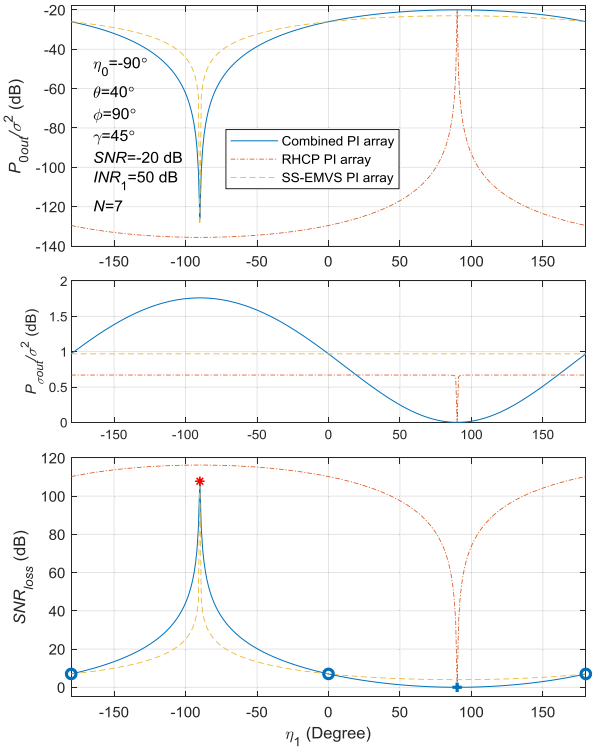

FIGURE 7. P_{0out}/σ^2, $P_{\sigma out}/\sigma^2$ and SNR_{loss} versus polarization angle η_1.

Figure 7 shows the normalized power P_{0out}/σ^2, $P_{\sigma out}/\sigma^2$ and SNR_{loss} versus polarization angle η_1 with the combined PI array, RHCP PI array and SS-EMVS PI array. The SNR is -20 dB, INR_1 is 50 dB and N is 7. All signals have $\theta = 40^\circ$, $\phi = 90^\circ$ and $\gamma = 45^\circ$, and η_1 of the interference signal is varied. In this figure, $*$ denotes the satellite signal, $+$ denotes the LHCP interferer, and $\bigcirc$ denotes the LP interferer. For the RHCP PI array, $\tilde{\boldsymbol{s}}_{sp\_sub1}^H \tilde{\boldsymbol{s}}_{sp\_sub0} = N s_{p\_ref1}^H$ and $\left\| \tilde{\boldsymbol{s}}_{sp\_sub1} \right\|^2 = N\alpha_1$. From (40), P_{0out}/σ^2 is approximately 0 for the RHCP PI array when $s_{p\_ref1} \neq 0$, i.e. $\eta_1 \neq 90^\circ$. Therefore, as long as $\eta_1 \neq 90^\circ$, the interference suppression results in significant SNR_{loss}. From Figure 7, the RHCP PI array can only acquire the satellite signal with $SNR_{loss} <$ 20 dB when the interference is LHCP. The combined PI array has a lower SNR_{loss} and a higher P_{0out}/σ^2 compared to the RHCP PI array. For an LP interference signal incident from

the same direction as the desired signal, SNR_{loss} with the combined PI array is approximately 7 dB. The satellite signal acquisition with LHCP interference is better than that with LP interference. However, when the polarization angle η_1 is close to η_0, SNR_{loss} increases rapidly. These results indicate that the combined PI array provides improved satellite signal acquisition in the polarization domain compared to the RHCP PI array. Further, the combined PI array has a lower P_{0out}/σ^2 but higher $P_{\sigma out}/\sigma^2$ than the SS-EMVS PI array with $\eta_1 < 0°$, which results in a greater SNR loss than the SS-EMVS PI array. Moreover, the satellite signal acquisition with the combined PI array is better than that with the SS-EMVS PI array when suppressing left-hand interference.

2) SIGNAL ACQUISITION IN SPATIAL DOMAIN

Assume that the interference has the same polarization angle as the satellite signal and $P_1 \gg \sigma^2$, and the number of subarray elements $N-1$ is a multiple of 3. For the combined PI array

$$\tilde{\boldsymbol{s}}_{sp\_sub1}^H \tilde{\boldsymbol{s}}_{sp\_sub0} = \tilde{\boldsymbol{s}}_{p\_sub1}^H diag\{\boldsymbol{D}\}\tilde{\boldsymbol{s}}_{p\_sub0} \tag{48}$$

with

$$\tilde{\boldsymbol{s}}_{p\_sub1}^H = \tilde{\boldsymbol{s}}_{p\_sub}^H(\theta_1, \phi_1, 45°, -90°) \tag{49}$$

$$\boldsymbol{D} = \tilde{\boldsymbol{s}}_{s\_sub}^H(\theta_1, \phi_1) \odot \tilde{\boldsymbol{s}}_{s\_sub}(\theta_0, \phi_0) \tag{50}$$

$$\tilde{\boldsymbol{s}}_{p\_sub0} = \tilde{\boldsymbol{s}}_{p\_sub}(\theta_0, \phi_0, 45°, -90°) \tag{51}$$

As $s_{p\_ref1} = s_{p\_ref0} = 1$ and $\alpha_1 = \alpha_0 = 1$, P_{0out} and $P_{\sigma out}$ can be approximated as

$$P_{0out} \approx P_0 \left| 1 - \frac{3}{N-1} \tilde{\boldsymbol{s}}_{p\_sub1}^H diag\{\boldsymbol{D}\}\tilde{\boldsymbol{s}}_{p\_sub0} \right|^2 \tag{52}$$

and

$$P_{\sigma out} \approx \sigma^2 \left[1 + \frac{3}{N-1} \right] \tag{53}$$

The SNR loss is given as

$$SNR_{loss} \approx 10 \log \frac{1 + \frac{3}{N-1}}{\left| 1 - \frac{3}{N-1} \tilde{\boldsymbol{s}}_{p\_sub1}^H diag\{\boldsymbol{D}\}\tilde{\boldsymbol{s}}_{p\_sub0} \right|^2} \text{ (dB)} \tag{54}$$

From (54), SNR_{loss} is a function of N, (θ_0, ϕ_0) and (θ_1, ϕ_1). When (θ_0, ϕ_0) is equal to (θ_1, ϕ_1), the value of $\tilde{\boldsymbol{s}}_{p\_sub1}^H diag\{\boldsymbol{D}\}\tilde{\boldsymbol{s}}_{p\_sub0}$ is equal to $(N-1)/3$, which results in an SNR loss approaching infinity. Besides, $P_{\sigma out}$ is determined by N and decreases as N increases. When (θ_0, ϕ_0) is not equal to (θ_1, ϕ_1), P_{0out} is greater than 0. Therefore, when the interference has the same polarization angles as the satellite signal, the array performs as space-only processing.

Figure 8 shows the normalized power P_{0out}/σ^2, $P_{\sigma out}/\sigma^2$ and SNR_{loss} versus θ_1 with the combined PI array, RHCP PI array and SS-EMVS PI array. The input SNR is -20 dB, INR_1 is 50 dB and N is 7. Assume that all signals have $\phi = 90°$, the pitch angle of the satellite signal is $\theta_0 = 40°$, and θ_1 of the interference signal is varied. When the pitch angle θ_1 is

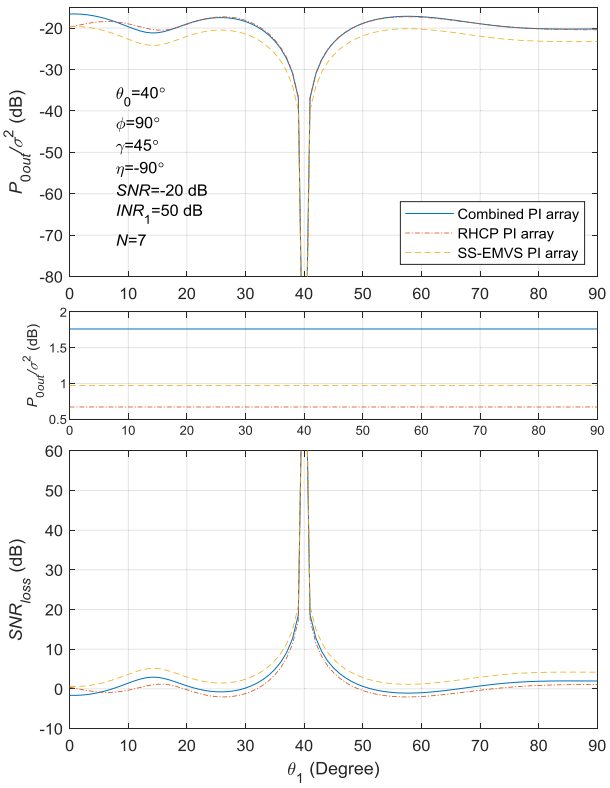

FIGURE 8. P_{0out}/σ^2, $P_{\sigma out}/\sigma^2$ and SNR_{loss} versus θ_1.

getting closer to θ_0, SNR loss increases rapidly for the three arrays. For the SS-EMVS PI array, $s_{p\_ref1}/s_{p\_ref0} = 1$ and $\alpha_0 = 1/2$. For the combined PI array, $s_{p\_ref1}/s_{p\_ref0} = 1$ and α_0=1. Thus from (41), P_{0out}/σ^2 of the SS-EMVS PI array is lower than the combined PI array due to the smaller α_0, which results in a lower SNR_{loss}. This indicates that better polarization matching with the satellite signal introduces less SNR loss. Further, the combined PI array has a P_{0out}/σ^2 close to that of the RHCP PI array. But the RHCP PI array has a lower $P_{\sigma out}/\sigma^2$ than the combined PI array due to the larger value of $\left\|\tilde{\boldsymbol{s}}_{sp\_sub1}\right\|^2$. In summary, the combined PI array retains the polarization matching with the satellite signal compared to the RHCP PI array, and provides improved satellite signal acquisition in the spatial domain compared to the SS-EMVS PI array.

3) SIGNAL ACQUISITION IN SPACE-POLARIZATION DOMAIN

Assume that the interference has both different polarization angle and DOA than the satellite signal, and all signals have $\phi = 90°$ and $\gamma = 45°$. The parameters of the satellite signal are set to $(\theta_0, \eta_0) = (40°, -90°)$ and the parameters of the interference signal (θ_1, η_1) are varied. The input $SNR$is -20 dB, INR_1 is 50 dB and N is 7. Figure 9 presents SNR_{loss} versus (θ_1, η_1) of the combined PI array. This shows that when the pitch angle θ_1 and polarization angle η_1 are the same as θ_0 and η_0, SNR_{loss} increases rapidly.

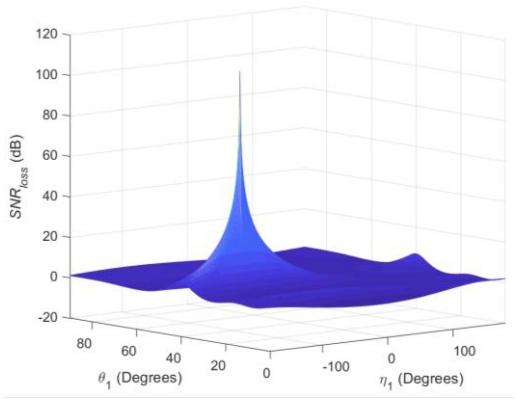

FIGURE 9. SNR_{loss} versus (θ_1, η_1) of the combined PI array.

Figure 10 shows the contour plot of SNR_{loss} for the combined PI array, RHCP PI array and SS-EMVS PI array. In Figure 10(a), $SNR_{loss} > 5$ dB for $35^{\circ} < \theta_1 < 45^{\circ}$ when $\eta_1 = \eta_0$ and $-180^{\circ} < \eta_1 < 10^{\circ}$ when $\theta_1 = \theta_0$. In Figure 10(b), $SNR_{loss} > 5$ dB for $36^{\circ} < \theta_1 < 43^{\circ}$ except $\eta_1 = 90^{\circ}$. Using the SS-EMVS subarray in the PI array reduces the SNR loss when the incident direction of the satellite signal is close to that of the interference compared to a traditional RHCP PI array. Figure 10(c) shows that the contour line with $SNR_{loss} = 5$ dB is similar to that in Figure 10(a), but the region of (θ_1, η_1) with $SNR_{loss} > 5$ dB is larger than in Figure 10(a). Using an RHCP reference antenna in the PI array reduces the SNR loss compared to the SS-EMVS PI array. From (41), this lower loss results from a larger value of α_0, which represents better polarization matching with the satellite signal. In summary, the combined PI array improves the satellite signal acquisition performance in the space-polarization domain compared to the RHCP PI array and the SS-EMVS PI array.

4) EFFECT OF THE NUMBER OF ELEMENTS AND INTERFERENCE PARAMETERS

From (40) to (43), SNR_{loss} for the PI array is determined by INR_1, $\boldsymbol{s}_{sp0}$ and $\boldsymbol{s}_{sp1}$.

Assume that all signals have $\phi = 90^{\circ}$ and $\gamma = 45^{\circ}$. The parameters of the desired signal are set to $(\theta_0, \eta_0) = (40^{\circ}, -90^{\circ})$. Figure 11 shows SNR_{loss} for different values of (θ_1, η_1) versus INR_1 and N for the three PI arrays. An LP interferer with $\theta_1 = 40^{\circ}$, LHCP interferer with $\theta_1 = 40^{\circ}$ and RHCP interferer with $\theta_1 = 20^{\circ}$ are considered in Figure 11(a). This indicates that when INR_1 is greater than 20 dB, SNR_{loss} does not change significantly with increasing INR_1 in all cases. When the interference is an LHCP signal incident from the same direction as the satellite signal, the combined PI array has the lowest SNR_{loss}. When the interference is an LP signal, SNR_{loss} increases as INR_1 increases from -20 dB to 20 dB for the combined PI array and SS-EMVS PI array, but the former array has a lowerSNR_{loss}. For an RHCP interferer incident from a different direction than the satellite signal, SNR_{loss} increases for the combined PI array and SS-EMVS PI array but decreases for the RHCP PI array as INR_1 increases from -20 dB to 20 dB. In this case, the combined PI array has the lowest SNR_{loss}.

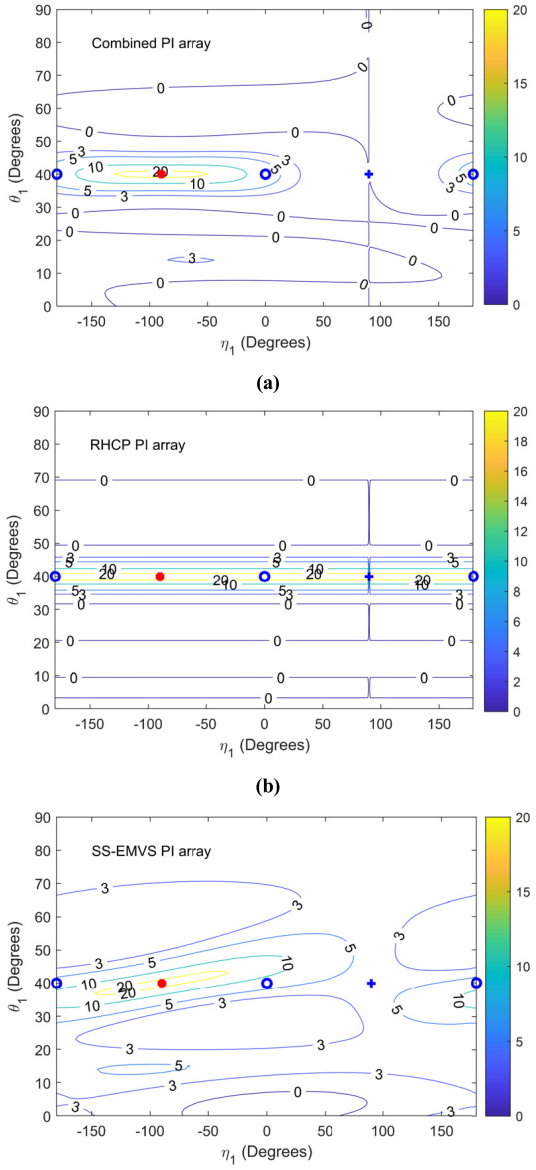

FIGURE 10. Contour plots of SNR_{loss} for the (a) combined PI array, (b) RHCP PI array, and (c) SS-EMVS PI array.

An LP interferer with $\theta_1 = 40^{\circ}$, LHCP interferer with $\theta_1 = 40^{\circ}$ and RHCP interferer with $\theta_1 = 35^{\circ}$ are considered in Figure 8(b). As the number of array elements N increases, SNR_{loss} decreases for all three arrays when the RHCP interference is incident close to the direction of the satellite signal. This is because a larger N results in higher array spatial resolution. With LHCP interference, SNR_{loss} does not change significantly as N increases for the combined PI array and RHCP PI array, but fluctuates for the SS-EMVS PI array. With LP interference, SNR_{loss} does not decrease

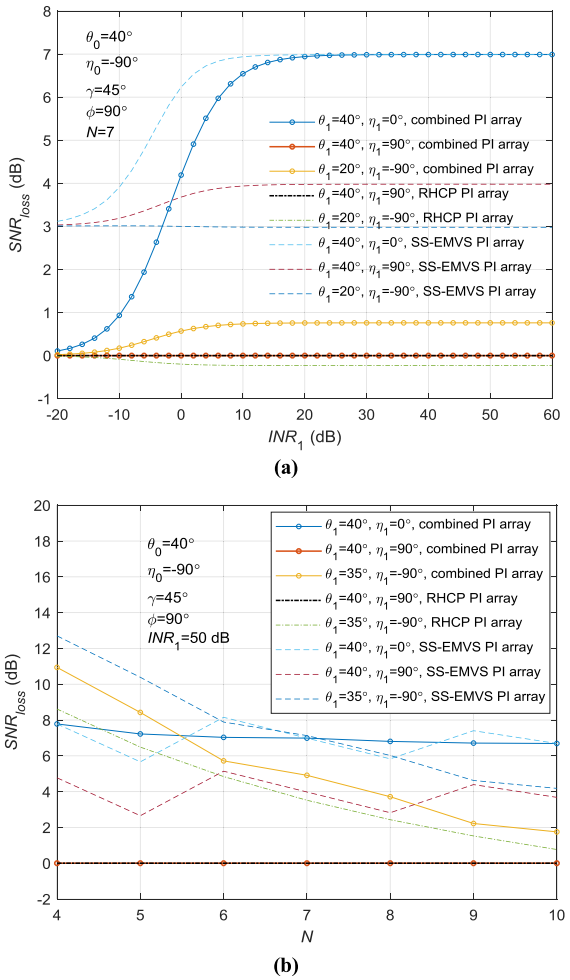

FIGURE 11. SNR_{loss} of the combined PI array, RHCP PI array and SS-EMVS PI array, (a) SNR_{loss} versus INR_1, and (b)SNR_{loss} versus the number of array elements N.

significantly for the combined PI array while it fluctuates for the SS-EMVS PI array. In general, a larger N improves the spatial resolution but not the polarization resolution for all arrays.

C. ROBUSTNESS ANALYSIS

In the previous analysis, a single interference signal incident on the array was considered. However, there could be no interferers or multiple interferers incident on the array. The robustness of the combined PI array under these two conditions is analyzed below.

1) NO INTERFERERS

$\boldsymbol{R}_3$ in (26) is $\boldsymbol{R}_3 = P_0\tilde{\boldsymbol{s}}_{sp\_sub0}\boldsymbol{s}^H_{p\_ref0}$ and $\tilde{\boldsymbol{R}}$ is $\tilde{\boldsymbol{R}} = P_0\tilde{\boldsymbol{s}}_{sp\_sub0}\tilde{\boldsymbol{s}}^H_{sp\_sub0} + \sigma^2\boldsymbol{E}_{N-1}$. From the matrix inversion lemma

$$\tilde{\boldsymbol{R}}^{-1} = \frac{1}{\sigma^2}[\boldsymbol{E}_{N-1} - \frac{SNR\tilde{\boldsymbol{s}}_{sp\_sub0}\tilde{\boldsymbol{s}}^H_{sp\_sub0}}{1 + SNR\left\|\tilde{\boldsymbol{s}}_{sp\_sub0}\right\|^2}] \tag{55}$$

where $\left\|\boldsymbol{s}_{p\_sub0}\right\|^2 = \boldsymbol{s}^H_{p\_sub0}\boldsymbol{s}_{p\_sub0}$. The satellite signal power and noise power at the output of the array are

$$P_{0out} = P_0\alpha_0\left(\frac{1}{1 + SNR\left\|\tilde{\boldsymbol{s}}_{sp\_sub0}\right\|^2}\right)^2 \tag{56}$$

$$P_{\sigma out} = \sigma^2\left[1 + \alpha_0\frac{SNR^2\left\|\tilde{\boldsymbol{s}}_{sp\_sub0}\right\|^2}{\left(1 + SNR\left\|\tilde{\boldsymbol{s}}_{sp\_sub0}\right\|^2\right)^2}\right] \tag{57}$$

The SNR loss is

$$SNR_{loss} = 10\lg\left[\frac{\left(1+SNR\left\|\tilde{\boldsymbol{s}}_{sp\_sub0}\right\|^2\right)^2}{\alpha_0} + SNR^2\left\|\tilde{\boldsymbol{s}}_{sp\_sub0}\right\|^2\right] \text{(dB)} \tag{58}$$

From (58), SNR_{loss} is determined by the input SNR, α_0 and $\left\|\tilde{\boldsymbol{s}}_{sp\_sub0}\right\|^2$. After some mathematical manipulation, we obtain

$$|E_{x0}|^2 = \left|E_x(\theta_0, \phi_0, 45°, -90°)\right|^2 = \frac{1}{2} - \frac{1}{2}\cos^2\phi_0\sin^2\theta_0 \tag{59}$$

Therefore, $\alpha_0 = |E_{x0}|^2 \le \frac{1}{2}$ for the SS-EMVS PI array which is less than the value of α_0 for the combined PI array. For the RHCP PI array, $\left\|\tilde{\boldsymbol{s}}_{sp\_sub0}\right\|^2 = N\alpha_0 = N$. The value of $\left\|\tilde{\boldsymbol{s}}_{sp\_sub0}\right\|^2$ is less than N for the combined PI array. SNR_{loss} is a monotonically decreasing function of $\left\|\tilde{\boldsymbol{s}}_{sp\_sub0}\right\|^2$ but a monotonically increasing function of α_0. Therefore, SNR_{loss} with the combined PI array is minimal for all (θ_0, ϕ_0) due to the lowest $\left\|\tilde{\boldsymbol{s}}_{sp\_sub0}\right\|^2$ and the largest α_0 compared to for the other two arrays.

In Figure 12, the azimuth angle of the satellite signal is set to $\phi_0 = 90°$. These results show that the SNR loss with the combined PI array is minimal for all values of θ_0, input SNR and number of elements N, which is consistent with the analysis. Figure 12(a) indicates that SNR_{loss} remains unchanged for the three arrays as θ_0 is varied. This results from α_0 is independent of θ_0 when $\phi_0 = 90°$ and $N = 7$. Figure 12(b) shows that SNR_{loss} increases as the input SNR increases for the three arrays. This is due to the PI algorithm suppressing high power signals as interference when there is no interference. Further, when the input SNR is lower than -25 dB, SNR_{loss} is close to 0 for the combined PI array and the RHCP PI array. Figure 12(c) indicates that SNR_{loss} increases as the number of array elements N increases for these three arrays. This is because the value of $\left\|\tilde{\boldsymbol{s}}_{sp\_sub0}\right\|^2$ increases as N increases. However, the increase in SNR_{loss} due to the increases in N is not significant for the combined PI array.

In summary, the combined PI array provides satellite signal acquisition with the lowest SNR loss compared to the other two PI arrays when there are no interferers. This loss increases with increasing input SNR and number of array

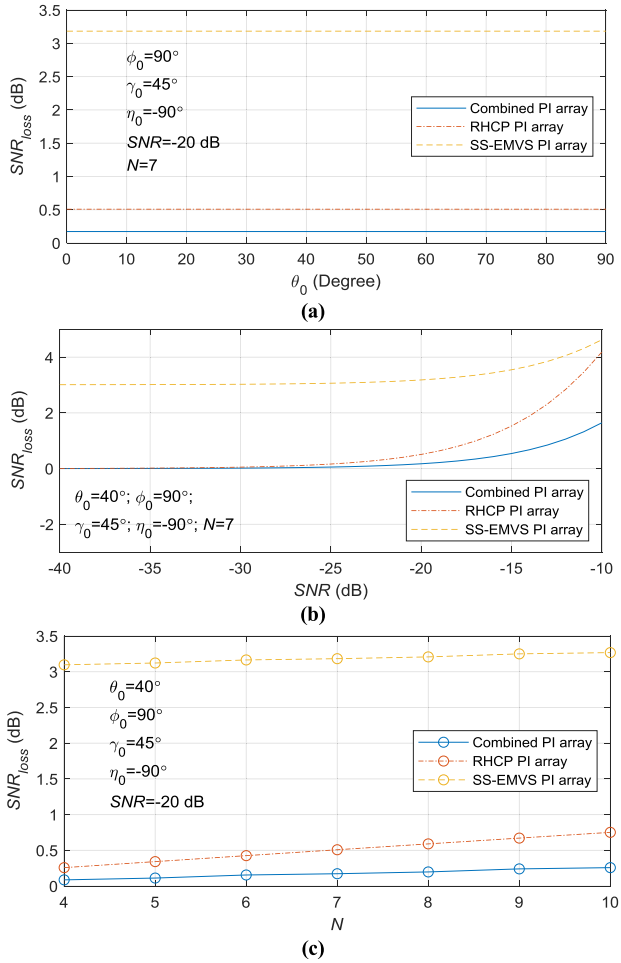

FIGURE 12. SNR_{loss} with no interferers, (a) SNR_{loss} versus θ_0, (b) SNR_{loss} versus input SNR, and (c) SNR_{loss} versus the number of elements$N$.

elements N. The SNR loss is less than 0.5 dB when input $SNR < -20$ dB, which can be considered as a minimal SNR loss.

2) MULTIPLE INTERFERERS

$\boldsymbol{R}_3$ and $\tilde{\boldsymbol{R}}$ in the presence of K interferers can be approximated as

$$\boldsymbol{R}_3 \approx \sum_{k=1}^{K} P_k \tilde{\boldsymbol{s}}_{sp\_subk} s_{p\_refk}^H \tag{60}$$

$$\tilde{\boldsymbol{R}} \approx \sigma^2 \boldsymbol{E}_{N-1} + \boldsymbol{S}_{sub} \boldsymbol{P} S_{sub}^H \tag{61}$$

where $\boldsymbol{S}_{sub} = [\tilde{\boldsymbol{s}}_{sp\_sub1}, \tilde{\boldsymbol{s}}_{sp\_subK}]$ and $\boldsymbol{P} = diag\{P_1, \cdots, P_K\}$. Assuming that P_k is much larger than σ^2, the first term in (61) can be ignored. Therefore, $\tilde{\boldsymbol{R}}^{-1}$ can be expressed as

$$\tilde{\boldsymbol{R}}^{-1} \approx (\boldsymbol{S}_{sub} \boldsymbol{P} S_{sub}^H)^{-1} = (\boldsymbol{S}_{sub}^+)^H \boldsymbol{P}^{-1} \boldsymbol{S}_{sub}^+ \tag{62}$$

The power of the ith interferer at the output of the array can be written as

$$\begin{aligned} P_{iout} &= E\left\{ \left| s_{p\_refi} I_i(t) + \tilde{\boldsymbol{w}}_{opt}^H \tilde{\boldsymbol{s}}_{sp\_subi} I_i(t) \right|^2 \right\} \\ &= P_i \left| s_{p\_refi} - \sum_{k=1}^{K} P_k s_{p\_refk} (\boldsymbol{S}_{sub}^+ \tilde{\boldsymbol{s}}_{sp\_subk})^H \right. \\ &\qquad \left. \boldsymbol{P}^{-1} \boldsymbol{S}_{sub}^+ \tilde{\boldsymbol{s}}_{sp\_subi} \right|^2 \end{aligned} \tag{63}$$

The pseudo-inverse matrix $\boldsymbol{S}_{sub}^+$ is such that

$$\boldsymbol{S}_{sub}^+ \tilde{\boldsymbol{s}}_{sp\_subi} = \left[\underbrace{0, 0, \cdots}_{i-1}, 1, \underbrace{0, \cdots, 0}_{K-i} \right]^T \tag{64}$$

and

$$(\boldsymbol{S}_{sub}^+ \tilde{\boldsymbol{s}}_{sp\_subj})^H \boldsymbol{P}^{-1} \boldsymbol{S}_{sub}^+ \tilde{\boldsymbol{s}}_{sp\_subi} = \begin{cases} \dfrac{1}{P_i}, & j = i \\ 0, & j \neq i \end{cases} \tag{65}$$

Substitute (64) and (65) into (63) gives

$$P_{iout} \approx P_i \left| s_{p\_refi} - s_{p\_refi} \right|^2 = 0 \tag{66}$$

Equation (66) indicates that the combined PI array can suppress each interference signal with corresponding output power approximately 0. In summary, the combined PI array provides satellite signal acquisition with a slight SNR loss when there are no interferers, and interference suppression for each interferer when there are multiple interferers. Therefore, the array is robust to various interference conditions.

IV. EXPERIMENT RESULTS FOR BDS PUBLIC SERVICE SIGNALS

In the previous analysis, the received signal was assumed to be approximately narrowband. In order to evaluate the interference suppression performance for the BDS public service signals more accurately, the received array signal is generated using time delay instead of phase delay as in (1). $\tilde{\boldsymbol{R}}$ and $\boldsymbol{R}_3$ for calculating $\boldsymbol{w}_{opt}$ are estimated from the available data using

$$\hat{\tilde{\boldsymbol{R}}} = \frac{1}{L} \sum_{l=1}^{L} \tilde{\boldsymbol{S}}_{sp}(l) \tilde{\boldsymbol{S}}_{sp}^H(l) \tag{67}$$

$$\hat{\boldsymbol{R}}_3 = \frac{1}{L} \sum_{l=1}^{L} \tilde{\boldsymbol{S}}_{sp}(l) S_{sp1}^H(l) \tag{68}$$

where L is the number of samples.

A. INTERFERENCE SCENARIOS

Table 1 gives the five interference scenarios which will be used to evaluate the performance of the combined PI array with the BDS B1I, B1C, B2a, and B3I signals. All interferers have INR=50 dB, $\phi = 90°$ and $\gamma = 45°$. The bandwidth of the frequency sweep signals is set to be the same as that of the satellite signal, and are mutually independent.

TABLE 2. Interference scenarios.

Scenario	Interference Type[a]	θ	η
1	Linear frequency sweep (Bandwidth=B, f_c=f_0)	60°	-90°
2	Linear frequency sweep (Bandwidth=B, f_c=f_0)	40°	0°
3	Single tone (f_c=f_0)	10°	-90°
	Linear frequency sweep (Bandwidth=B, f_c=f_0)	60°	-90°
4	Single tone (f_c=f_0)	10°	50°
	Single tone (f_c=f_0+1 MHz)	70°	-20°
	Linear frequency sweep (Bandwidth=B, f_c=f_0)	55°	120°
	Sinusoidal frequency sweep (Bandwidth=B, f_c=f_0)	90°	-100°
5	Single tone (f_c=f_0)	10°	50°
	Single tone (f_c=f_0+1 MHz)	70°	-20°
	Single tone (f_c=f_0-1 MHz)	20°	0°
	Linear frequency sweep (Bandwidth=B, f_c=f_0)	55°	120°
	Sinusoidal frequency sweep (Bandwidth=B, f_c=f_0)	90°	-100°
	Logarithmic frequency sweep (Bandwidth=B, f_c=f_0)	30°	90°
	Exponential frequency sweep (Bandwidth=B, f_c=f_0)	60°	150°

[a]Values of B and f_0 for BDS B1I, B1C, B2a, B3I signals are shown in Table 1. The period of the frequency sweep signals is 1 ms, and f_c is the frequency of the single tone interferers as well as the center frequency of the frequency sweep interferers.

B. EVALUATION METRICS

The signal to interference plus noise ratio (SINR) is a measure of the signal quality when interference is present [1]. It reflects the array performance for interference suppression and BDS signal acquisition. The output SINR of the combined PI array after interference suppression is

$$SINR = \frac{\boldsymbol{w}_{opt}^H \boldsymbol{R}_s \boldsymbol{w}_{opt}}{\boldsymbol{w}_{opt}^H (\boldsymbol{R}_i + \boldsymbol{R}_n) \boldsymbol{w}_{opt}} \tag{69}$$

The purpose of acquiring a satellite signal is to use it for measurements. Even if a BDS signal is acquired with an SINR which can meet the availability requirements of the receiver, the weighting and summation in (40) may affect the measurement result. The pseudorange measurement is widely used for BDS signals. It is based on extracting amplitude features of the cross-correlation (CC) between a BDS signal and the ranging code [27]. The corresponding measurement error is called the distortion metric (DM) [29]. The CC amplitude of the BDS signal at the array output is

$$|CC(\delta)| = \left| \frac{1}{L} \sum_{l=1}^{L} S_{BDSout}(l) e^{-j2\pi f_0 l/f_s} C_{BDS}(l-\delta) \right| \tag{70}$$

where f_s is sampling rate, C_{BDS} is the BDS ranging code, δ is the chip shift, and $S_{BDSout}(l)e^{-j2\pi f_0 l/f_s}$ represents the removal of the carrier. The clean CC amplitude (with $S_{BDS}(t)$) for the BDS B1I, B2a, B3I signals are triangular as shown in Figure 13(a). The mid abscissa value of the line connecting points with a normalized correlation of 0.5 on the Early and Late arms is denoted as the Prompt chip shift. The DM is the difference in the Prompt chip shifts for the clean CC amplitude and the amplitude after interference suppression. The B1C signal employs BOC and QMBOC modulation, so its CC amplitude is not triangular as shown in Figure 13(b). The portions with normalized correlation less than zero are called side peaks. The side peaks are typically eliminated during signal tracking in the receiver [30]. Therefore, the main peak with a normalized correlation greater than zero is used to calculate the DM using the approach shown in Figure 13(a).

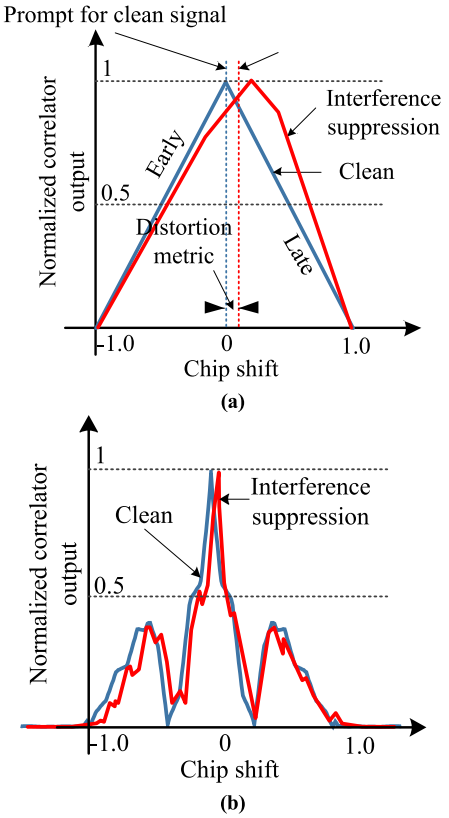

FIGURE 13. The CC amplitude distortion metric (DM) for (a) the B1I, B2a, and B3I signals and (b) the B1C signal.

C. PERFORMANCE EVALUATION

The minimum received power level is −163 dBW for the B1I signal, −159 dBW for the B1C signal, −156 dBW for the B2a signal and −163 dBW for the B3I signal. At an ambient temperature of 290 K, the noise power for a bandwidth B is [27]

$$\sigma^2 = N_0 B = 4 \times 10^{-21} \times B \tag{71}$$

where N_0 is the power spectral density of the white Gaussian noise. Thus, the noise power is −137.86 dBW, −128.83 dBW, −130.87 dBW and −130.87 dBW for the B1I, B1C, B2a and B3I signals, respectively, which is approximately −25 dB, −30 dB, −25 dB, −32 dB higher than the minimum received power of the satellite signals.

The input *SNR* is set to −20 dB, −25 dB, −20 dB and −27 dB for the B1I, B1C, B2a and B3I signals, respectively. The number of array elements is N =7. All signals have $\phi = 90°$ and $\gamma = 45°$, and the parameters of the desired signal are set to $(\theta_0, \eta_0) = (40°, -90°)$. Complex samples of the satellite signals, interference and noise were generated via simulation. The sampling rates were 20.23 MHz, 71.61 MHz, 51.15 MHz and 51.15MHz for the B1I, B1C, B2a and B3I signals, respectively. The output SINRs were obtained based on samples with the ranging code periods which are 1 ms for B1I, B2a, B3I signals and 10 ms for B1C signals.

Define the SINR loss as

$$SINR_{\text{loss}} = SINR_0 - SINR \tag{72}$$

where $SINR_0$ represents the output *SINR* with no interferers and is equal to the input *SNR*.

Figure 14(a) shows the output *SINR* for the five scenarios. When there are no interferers, the output *SINR* is approximately equal to the input SNR. When there is RHCP frequency sweep interference with $\theta = 60°$ incident on the array, the SINR loss is greater for the B1I signal than the other signals. The scenario 2 results indicate that the array suppresses an LP frequency sweep interference with $\theta = 40°$ and an SINR loss of approximately 7 dB, which is consistent with the SNR loss obtained via analysis. The scenario 3 results indicate that the array can simultaneously suppress RHCP single tone interference with $\theta = 20°$ and RHCP frequency sweep interference with $\theta = 60°$. The SINR loss is approximately 3 dB for the B1C, B2a, and B3I signals, and 5 dB for the B1I signal. Scenario 4 has four interference signals with different DOAs and polarization states. The B1I signal has the largest SINR loss of 5.5 dB, while the loss for the other signals is less than 3 dB. The results for scenario 5 indicate that when the number of interferers is equal to the number of array elements N, the SINR loss is greater than 25 dB. In summary, the combined PI array suppresses interference for all BDS public service signals with an SINR loss of less than 7 dB in scenarios 1 to 4. The array provides higher output SINRs with the B1C, B2a and B3I signals than the B1I signal.

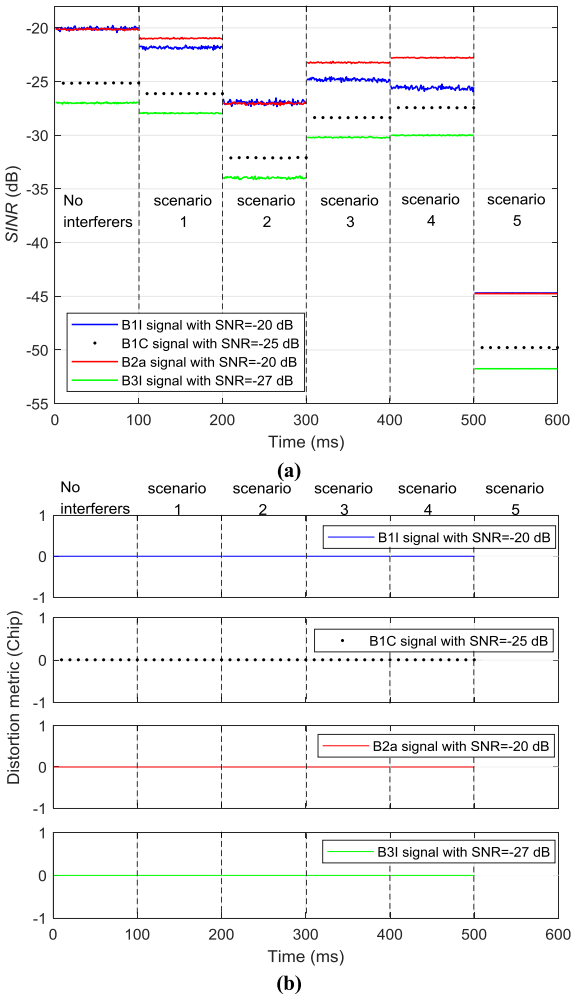

FIGURE 14. Interference suppression performance in different scenarios, (a) *SINR* and (b) the distortion metric.

Figure 14(b) shows the distortion metric for the output BDS signals for the five scenarios. Scenario 5 has an SINR lower than −50 dB, so the BDS signal could not be acquired and thus the distortion metric is meaningless. The distortion metrics for the B1I, B1C, B2a and B3I signals are all 0 in the remaining scenarios. From (40), when the signal is considered as narrowband, $S_{BDSout}(t)$ is the product of $S_{BDS}(t)$ and a complex coefficient. Thus from (70), the shape and chip shift of the CC amplitude for $S_{BDSout}(t)$ is not changed compared to $S_{BDS}(t)$. These results justify the narrowband assumption for BDS signals. The weights used with the BDS signals for interference suppression do not distort the CC amplitude, so there are no errors in the pseudorange measurements. In summary, the combined PI array is effective for interference suppression and satellite signal acquisition of all Beidou satellite system public service signals.

D. COMPUTATIONAL COMPLEXITY

The following four steps are needed to calculate $\tilde{\boldsymbol{w}}_{opt}$.

1) Calculate $\tilde{\boldsymbol{R}}$.
2) Calculate $\boldsymbol{R}_3$.
3) Calculate the inverse matrix of $\tilde{\boldsymbol{R}}$.
4) Calculate the product of $\tilde{\boldsymbol{R}}^{-1}$ and $\boldsymbol{R}_3$.

The number of computations for each step and the total number of computations are given in Table 3. It can be seen that an increase in L increases the number of real multiplications and divisions. In addition, for the same number of subarray elements, the number of computations for the combined PI array, RHCP PI array and SS-EMVS are equal. In other words, the proposed PI array does not increase the computational complexity of interference suppression.

For traditional PI arrays, iterative algorithms can be used to reduce the computational complexity, for example the Least Mean Square (LMS) algorithm [1]. The LMS algorithm computational complexity is $O\{N\}$ each iteration. This method can be implemented for the combined PI array in a way

TABLE 3. Number of computations to obtain the optimal weight vector.

Step	Real multiplications	Real divisions	Real additions
1	$4(N\text{-}1)^2L$	$2(N\text{-}1)^2$	$4(N\text{-}1)^2L\text{-}2(N\text{-}1)^2$
2	$4(N\text{-}1)L$	$2(N\text{-}1)$	$4(N\text{-}1)L\text{-}2(N\text{-}1)$
3[a]	$4(N\text{-}1)^3\text{-}2(N\text{-}1)^2$	$4(N\text{-}1)^2$	$4(N\text{-}1)^3\text{-}2(N\text{-}1)^2$
4	$4(N\text{-}1)^2$	0	$4(N\text{-}1)^2\text{-}2(N\text{-}1)$
Total	$4(N\text{-}1)^3+4(N\text{-}1)L$ $+2(N\text{-}1)^2$	$6(N\text{-}1)^2$ $+2(N\text{-}1)$	$4(N\text{-}1)^3+4(N\text{-}1)^2L$ $+4(N\text{-}1)L\text{-}4(N\text{-}1)$

[a]The computations listed were obtained considering Gaussian elimination. In general, the computational complexity for matrix inversion is $O\{N^3\}$ [31].

similar to that for traditional PI arrays, and so is not discussed here.

V. CONCLUSION

In this paper, a novel power inversion antenna array composed of an RHCP antenna and an SS-EMVS subarray was proposed. Replacing the subarray of the traditional RHCP PI array with an SS-EMVS subarray reduces the SNR degradation when the incident direction of a satellite signal is close to that of the interference. An RHCP element is used as a reference to ensure polarization matching with satellite signals. It was shown that the combined PI array can suppress interference and acquire satellite signals in both the spatial and polarization domains. The array provides better polarization domain performance than an RHCP PI array and has a lower SNR loss than an SS-EMVS PI array without increasing the computational complexity. The interference suppression effectiveness was demonstrated for BDS public service signals. Further, the proposed PI array introduces no errors in the pseudorange measurements.

REFERENCES

[1] R. T. Compton, "The power-inversion adaptive array: Concept and performance," *IEEE Trans. Aerosp. Electron. Syst.*, vol. 15, no. 6, pp. 803–814, Nov. 1979. doi: 10.1109/TAES.1979.308765.

[2] Y. Wan, F. Chen, J. Nie, and G. Sun, "Optimum reference element selection for GNSS power-inversion adaptive arrays," *Electron. Lett.*, vol. 52, no. 20, pp. 1723–1725, Sep. 2016. doi: 10.1049/el.2016.2360.

[3] H. Xu, X. Cui, and M. Lu, "Effects of power inversion spatial only adaptive array on GNSS receiver measurements," *Tsinghua Sci. Technol.*, vol. 23, no. 2, pp. 172–183, Apr. 2018. doi: 10.26599./TST.2018.9010019.

[4] China Satellite Navigation Office. (Nov. 2016). *BeiDou Navigation Satellite System Signal in Space: Interface Control Document, Open Service Signal, Version 2.1*. [Online]. Available: http://www.beidou.gov.cn/xt/gfxz/201805/P020180507527106075323.pdf

[5] China Satellite Navigation Office. (Dec. 2017). *BeiDou Navigation Satellite System Signal in Space: Interface Control Document, Open Service Signal B1C, Version 1.0*. [Online]. Available: http://www.beidou.gov.cn/xt/gfxz/201712/P020171226741342013031.pdf

[6] China Satellite Navigation Office. (Dec. 2017). *BeiDou Navigation Satellite System Signal in Space: Interface Control Document, Open Service Signal B2a, Version 1.0*. [Online]. Available: http://www.beidou.gov.cn/xt/gfxz/201712/P020171226742357364174.pdf

[7] China Satellite Navigation Office. (Feb. 2018). *BeiDou Navigation Satellite System Signal in Space: Interface Control Document, Open Service Signal B3I, Version 1.0*. [Online]. Available: http://www.beidou.gov.cn/xt/gfxz/201802/P020180209623601401189.pdf

[8] C. Sun, "Analysis and design of anti-jamming adaptive antenna array for satellite navigation system and HF antenna tuner," Ph.D. dissertation, School Electron. Eng., Xidian Univ., Xi'an, China, 2016.

[9] A. Narbudowicz, M. J. Ammann, and D. Heberling, "Reconfigurable axial ratio in compact GNSS antennas," *IEEE Trans. Antennas Propag.*, vol. 64, no. 10, pp. 4530–4533, Oct. 2016. doi: 10.1109/TAP.2016.2589975.

[10] C. Wei, J. Liu, F. Zhang, and P. Liu, "The comparison of two adaptive anti-jamming algorithm of navigation receiver," in *Proc. China Satellite Navigat. Conf. (CSNC)*, in Lecture Notes in Electrical Engineering, vol. 161. Berlin, Germany: Springer, 2012, pp. 591–600.

[11] H. Zhao, Y. Shi, B. Zhang, and M. Shi, "Analysis and simulation of interference suppression for space-time adaptive processing," in *Proc. IEEE Int. Conf. Signal Process., Commun. Comput.*, Guilin, China, Aug. 2014, pp. 724–727.

[12] X. Dai, J. Nie, F. Chen, and G. Ou, "Distortionless space-time adaptive processor based on MVDR beamformer for GNSS receiver," *IET Radar Sonar Navigat.*, vol. 11, no. 10, pp. 1488–1494, Sep. 2017. doi: 10.1049/iet-rsn.2017.0168.

[13] M. Yang, J. Ding, B. Chen, and X. Yuan, "A multiscale sparse array of spatially spread electromagnetic-vector-sensors for direction finding and polarization estimation," *IEEE Access*, vol. 6, pp. 9807–9818, Jan. 2018. doi: 10.1109/ACCESS.2018.2799905.

[14] N. Wu, Z. Qu, W. Si, and S. Jiao, "DOA and polarization estimation using an electromagnetic vector sensor uniform circular array based on the ESPRIT algorithm," *Sensors*, vol. 16, no. 12, pp. 1–20, Dec. 2016. doi: 10.3390/s16122109.

[15] G. Zheng, "Two-dimensional DOA estimation for polarization sensitive array consisted of spatially spread crossed-dipole," *IEEE Sensors J.*, vol. 18, no. 12, pp. 5014–5023, Jun. 2018. doi: 10.1109/JSEN.2018.2820168.

[16] Z. Xu, L. Zhang, D. Wu, Z. Xiong, and S. Xiao, "Filtering performance of alternate polarization array," *J. Nat. Univ. Defense Technol.*, vol. 34, no. 5, pp. 49–54, Sep. 2012. doi: 10.3969/j.issn.1001-2486.2012.05.011.

[17] B. Li, W. Bai, and G. Zheng, "Successive ESPRIT algorithm for joint DOA-range-polarization estimation with polarization sensitive FDA-MIMO radar," *IEEE Access*, vol. 6, pp. 36376–36382, 2018. doi: 10.1109/ACCESS.2018.2844948.

[18] S. Gong, C. Xing, S. Chen, and Z. Fei, "Polarization sensitive array based physical-layer security," *IEEE Trans. Veh. Technol.*, vol. 69, no. 5, pp. 3964–3981, May 2018. doi: 10.1109/TVT.2017.2773710.

[19] D. Wu, Z.-H. Xu, Z. Xiong, L. Zhang, and S. Xiao, "Performance analysis of polarization-space-time joint domain processing for clutter suppression in airborne radars," *Acta Electrica Sinica*, vol. 40, no. 7, pp. 1429–1433, Jul. 2012. doi: 10.3969/j.issn.0372-2112.2012.07.023.

[20] G. Zheng and B. Wu, "Polarisation smoothing for coherent source direction finding with multiple-input and multiple-output electromagnetic vector sensor array," *IET Signal Process.*, vol. 10, no. 8, pp. 873–879, Oct. 2016. doi: 10.1049/iet-spr.2015.0535.

[21] L. Sun, "Research on anti-jamming and multipath mitigation by reduced distributed vector sensor in satellite navigation systems," Ph.D. dissertation, Dept. Satell. Navigat. Positioning R&D Center, School Electron. Sci. Eng., Nat. Univ. Defense Technol., Changsha, China, 2011.

[22] W. Zeng, L. Wang, Y. Wang, Z. Zhang, and M. Zhang, "Joint polarized and spatial domain anti-jamming method for GNSS," in *Proc. IEEE Int. Conf. Signal Process., Commun. Comput.*, Kunming, China, Aug. 2013, pp. 1–5.

[23] H. Wang, L. Yang, Y. Yang, and H. Zhang, "Anti-jamming of Beidou navigation based on polarization sensitive array," in *Proc. Int. Appl. Comput. Electromagn. Soc. Symp.*, Suzhou, China, Aug. 2017, pp. 1–2.

[24] L. Sun, J. Chen, S. Tan, and Z. Chai, "Research on multipath limiting antenna array with fixed phase center," *GPS Solutions*, vol. 19, no. 4, pp. 505–510, Oct. 2015. doi: 10.1007/s10291-014-0400-x.

[25] K.-C. Ho, K.-C. Tan, and K.-C. Tan, "Linear dependence of steering vectors associated with tripole arrays," *IEEE Trans. Antennas Propag.*, vol. 46, no. 11, pp. 1705–1711, Nov. 1998. doi: 10.1109/8.736626.

[26] X. Zhang, F. Wang, and D. Xu, *Theory and Application of Array Signal Processing*. Beijing, China: National Defense Industry Press, 2013, pp. 185–186.

[27] G. Z. Xie, *Principles of GPS and Receiver Design*. Beijing, China: Publishing House of Electronics Industry, 2014, pp. 244–246.

[28] S. Zhong, *Electromagnetic Fields and Waves*. Beijing, China: Tsinghua Univ. Press, 2006, pp. 155–159.

[29] T. Marathe, S. Daneshmand, and G. Lachapelle, "Assessment of measurement distortions in GNSS antenna array space-time processing," *Int. J. Antennas Propag.*, vol. 1, no. 2, pp. 1–17, Feb. 2016. doi: 10.1155/2016/2154763.

[30] B. Zu, "Research on the key techniques of Compass-M1 civilian software receiver," Ph.D. dissertation, School Automat., Harbin Inst. Technol., Harbin, China, 2010.
[31] L. Dong, "Matrix inversion implementation based on joint space-time anti-jamming algorithm," *Telecommun. Eng.*, vol. 55, no. 7, pp. 792–796, Jul. 2015. doi: 10.3969/j.issn.1001.893x.2015.07.015.

YIHENG JIN was born in Shandong, China, in 1992. She received the B.S. degree in communication engineering from the Ocean University of China, in 2013, where she is currently pursuing the Ph.D. degree with the Department of Electronic Engineering. Her research interests include GNSS anti-interference techniques, adaptive antenna arrays, GNSS high accuracy positioning, and spread spectrum communications.

HAO ZHANG (SM'13) was born in Jiangsu, China, in 1975. He received the B.S. degree in telecom engineering and industrial management from Shanghai Jiao Tong University, China, in 1994, the M.B.A. degree from the New York Institute of Technology, New York, NY, USA, in 2001, and the Ph.D. degree in electrical engineering from the University of Victoria, Victoria, BC, Canada, in 2004. From 1994 to 1997, he was Assistant President of ICO (China) Global Communications Company. He is currently a Professor with the Department of Electrical Engineering, Ocean University of China. He is also an Adjunct Professor with the Department of Electrical and Computer Engineering, University of Victoria. His research interests include ultra-wideband systems, MIMO wireless systems, and spread spectrum communications.

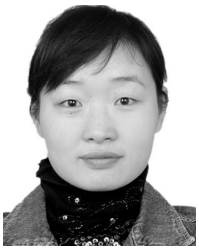

TINGTING LU was born in 1983. She received the B.S. degree in communication engineering from Hunan University, in 2006, and the M.S. degree in communication and information systems and the Ph.D. degree in computer application technology from the Ocean University of China, in 2009 and 2013, respectively, where she is a currently a Lecturer. Her research interests include mmWave communication systems, MIMO wireless systems, OFDM technologies, and GNSS.

HUA YANG received the M.S. degree from Shandong University and the Ph.D. from Shanghai Jiao Tong University, Shanghai, China. She is currently an Associate Professor with the Information Science and Engineering College, Ocean University of China, Qingdao, China. She also serves as the Principal Investigator of the National Nature Science Foundation of China. Her research interests include wireless signals modeling and recognition, and the development of electronic products and systems.

T. AARON GULLIVER (S'81–M'90–SM'96) received the B.S. and M.Sc. degrees in electrical engineering from the University of New Brunswick, Fredericton, NB, Canada, in 1982 and 1984, respectively, and the Ph.D. degree in electrical and computer engineering from the University of Victoria, Victoria, BC, Canada, in 1989. From 1989 to 1991, he was employed as a Defence Scientist at the Defence Research Establishment Ottawa, Ottawa, ON, Canada. He has held academic positions at Carleton University, Ottawa, and the University of Canterbury, Christchurch, New Zealand. He joined the University of Victoria, in 1999, where he is currently a Professor with the Department of Electrical and Computer Engineering. His research interests include information theory and communication theory, algebraic coding theory, cryptography and security, and smart grid and ultra wideband communications. In 2002, he became a Fellow of the Engineering Institute of Canada, and a Fellow of the Canadian Academy of Engineering, in 2012.